



The preserved plume of the Caribbean Large Igneous Plateau revealed by 3D data-integrative models

Ángela María Gómez-García^{1,2,3,✉}, Eline Le Breton⁴, Magdalena Scheck-Wenderoth¹, Gaspar Monsalve², and Denis Anikiev¹

¹GFZ German Research Centre for Geosciences, 14473 Potsdam, Germany

²Facultad de Minas, Universidad Nacional de Colombia, Medellín, Colombia

³CEMarin – Corporation Center of Excellence in Marine Sciences, Bogotá, Colombia

⁴Institute of Geological Sciences, Freie Universität Berlin, 12249 Berlin, Germany

✉ *Invited contribution by Ángela María Gómez-García, recipient of the EGU Seismology Outstanding Student Poster and PICO Award 2019.*

Correspondence: Ángela María Gómez-García (angela@gfz-potsdam.de)

Received: 4 September 2020 – Discussion started: 28 September 2020

Revised: 19 November 2020 – Accepted: 4 December 2020 – Published: 29 January 2021

Abstract. Remnants of the Caribbean Large Igneous Plateau (C-LIP) are found as thicker than normal oceanic crust in the Caribbean Sea that formed during rapid pulses of magmatic activity at ~ 91 – 88 and ~ 76 Ma. Strong geochemical evidence supports the hypothesis that the C-LIP formed due to melting of the plume head of the Galápagos hotspot, which interacted with the Farallon (Proto-Caribbean) plate in the eastern Pacific. Considering plate tectonics theory, it is expected that the lithospheric portion of the plume-related material migrated within the Proto-Caribbean plate in a north–north-eastward direction, developing the present-day Caribbean plate. In this research, we used 3D lithospheric-scale, data-integrative models of the current Caribbean plate setting to reveal, for the first time, the presence of positive density anomalies in the uppermost lithospheric mantle. These models are based on the integration of up-to-date geophysical datasets from the Earth’s surface down to 200 km depth, which are validated using high-resolution free-air gravity measurements. Based on the gravity residuals (modelled minus observed gravity), we derive density heterogeneities both in the crystalline crust and the uppermost oceanic mantle (< 50 km). Our results reveal the presence of two positive mantle density anomalies beneath the Colombian and the Venezuelan basins, interpreted as the preserved fossil plume conduits associated with the C-LIP formation. Such mantle bodies have never been identified before, but a positive density trend is also indicated by S-wave

tomography, at least down to 75 km depth. The interpreted plume conduits spatially correlate with the thinner crustal regions present in both basins; therefore, we propose a modification to the commonly accepted tectonic model of the Caribbean, suggesting that the thinner domains correspond to the centres of uplift due to the inflow of the hot, buoyant plume head. Finally, using six different kinematic models, we test the hypothesis that the C-LIP originated above the Galápagos hotspot; however, misfits of up to ~ 3000 km are found between the present-day hotspot location and the mantle anomalies, reconstructed back to 90 Ma. Therefore, we shed light on possible sources of error responsible for this offset and discuss two possible interpretations: (1) the Galápagos hotspot migrated (~ 1200 – 3000 km) westward while the Caribbean plate moved to the north, or (2) the C-LIP was formed by a different plume, which – if considered fixed – would be nowadays located below the South American continent.

1 Introduction

Oceanic plateaus are vast areas characterized by a thicker than “normal” oceanic crust, which might reach up to 38 km (Kerr and Mahoney, 2007). Although about 12 different oceanic plateaus have been recognized worldwide, they represent one of the least well-known of Earth’s magmatic pro-

cesses (Kerr, 2014). In the early 1970s, Edgar et al. (1971) and Donnelly (1973) discovered the Caribbean Large Igneous Plateau, which corresponds to the second largest plateau (by area) after the Ontong Java Plateau, with an approximated extent of $1.1 \times 10^6 \text{ km}^2$ and an estimated excess magma volume of $4.4 \times 10^6 \text{ km}^3$ (Kerr, 2014).

The origin of such a vast volume of basalt is widely recognized as the interaction of a mantle plume with the over-riding, mobile lithosphere. With time, the plume-related material suffers physical and chemical changes, which at the same time are associated with a diversification in the way the plume interacts with the overriding plate. During the lifespan of a plume it is expected to first create extensive oceanic plateaus, followed by aseismic ridges, due to melting of the large plume head or the narrower plume tail, respectively (Campbell, 2005). The initial stages of the plume–lithosphere interaction include the uplift and weakening of the overlying lithosphere due to the inflow of hot, highly buoyant mantle material. At a later stage, when the plume is no longer active, geodynamic models show that the frozen plume material can be preserved into the lithosphere, forming high-density and therefore high-velocity bodies (François et al., 2018).

Successful detections of present-day mantle plumes using P-wave and/or S-wave velocity anomalies include the work of, for example, Montelli et al. (2004) and Civiero et al. (2019). These results suggest that the currently active plumes are characterized by negative velocity anomalies, associated with the presence of high-temperature material. The plume conduct shows a variety of shapes, some of which include the interconnection of branches at different depths (e.g. Civiero et al., 2019, and references therein). Imaging these complex systems, however, has posed a large challenge in the scientific community, especially for the correct interpretation of tomographic images (Campbell, 2005; Civiero et al., 2019).

The oceanic plateaus are normally difficult to subduct due to their abnormal thickness and positive thermal imprint inherited from their mantle plume origin. Thus, fragments of the Caribbean plateau have been accreted along continental margins, such as in Ecuador, Colombia, Panama, Costa Rica, Curaçao, and Hispaniola (Hastie and Kerr, 2010; Thompson et al., 2004). Using accreted material and relatively few drilled or dragged submarine rock samples, the geochemistry of the Caribbean Large Igneous Plateau (C-LIP) has been reconstructed (e.g. Geldmacher et al., 2003; Hastie and Kerr, 2010; Kerr and Tarney, 2005; Thompson et al., 2004). Indeed, strong geochemical evidence suggests that the C-LIP corresponds to melting of the plume head of the Galápagos hotspot (Geldmacher et al., 2003; Thompson et al., 2004), although recent kinematic reconstructions of the Caribbean do not allow us to trace back the location of the plate above the present-day location of the Galápagos plume (Boschman et al., 2014). Nevertheless, diverse evidence exists about the north–north-eastward migration of the Caribbean plate from

the eastern Pacific. The present-day Caribbean plate is composed of different accreted crustal domains (e.g. volcanic arcs, continental and oceanic realms) that have migrated since the Late Jurassic to Early Cretaceous period, including the igneous plateau materials that affected the oceanic crust of the former Farallon plate (Boschman et al., 2014; Montes et al., 2019a).

Different regions of the Caribbean have been the target of relatively extensive seismic reflection and refraction, sonar, and drilling campaigns (e.g. Diebold and Driscoll, 1999; Edgar et al., 1971; Kroehler et al., 2011; Mauffret and Leroy, 1997; Rosencrantz, 1990); some of which were undertaken with the limitations of early seismic acquisition technology. Nonetheless, the coverage of these measurements is poor when compared with the complexity of most of the Caribbean morphological structures.

In this paper, the main goal is to evaluate the present-day 3D lithospheric structure of the South Caribbean margin (continental and oceanic domains – black box in Fig. 1) by means of modelling of the gravity anomalies (Gz), which are especially sensitive to deep density distributions (Álvarez et al., 2014, 2015) and are therefore a potential tool for analysing the upper 200 km of the Earth. Here, the high spatial resolution EIGEN6C-4 dataset is used (Förste et al., 2014; Ince et al., 2019), which includes a spherical harmonic solution of up to a degree and order of $N_{\text{max}} = 2190$, equivalent to a topographic wavelength of $\sim 18 \text{ km}$.

Due to the fact that the gravity response of a system is the superposition of the gravity effects caused by all the density contrasts within it, we considered the gravitational effects caused by the heterogeneous lithospheric mantle in the South Caribbean and north-western South American plates. Therefore, the geometries of both the Nazca and the Caribbean flat slabs were included in the gravity models.

Previous studies in this region include few 3D lithospheric-scale, gravity-validated models (Gómez-García et al., 2019b; Sanchez-Rojas and Palma, 2014). However, some limitations of these attempts include, for instance, a spatially heterogeneous gravity dataset, a mantle that is considered to have a uniform and constant density, and that the analysis is of only the shallow density contrasts.

The results of the gravity inversion not only highlight crustal areas heavily affected by the high-density plume material but also suggest the presence of a high-density trend in the oceanic mantle of the Caribbean plate. This trend can be followed from the Moho down to 75 km depth, as supported by high S-wave velocities in the tomographic model SL2013sv (Schaeffer and Lebedev, 2013). These results are interpreted as the preserved, lithospheric fossil plume conduits, responsible for the development of the C-LIP, which migrated as the Proto-Caribbean lithosphere moved from the eastern Pacific.

Finally, taking advantage of the more precise spatial location of the C-LIP fossil plume conduits, different kinematic reconstructions are explored, aiming to evaluate the hypoth-

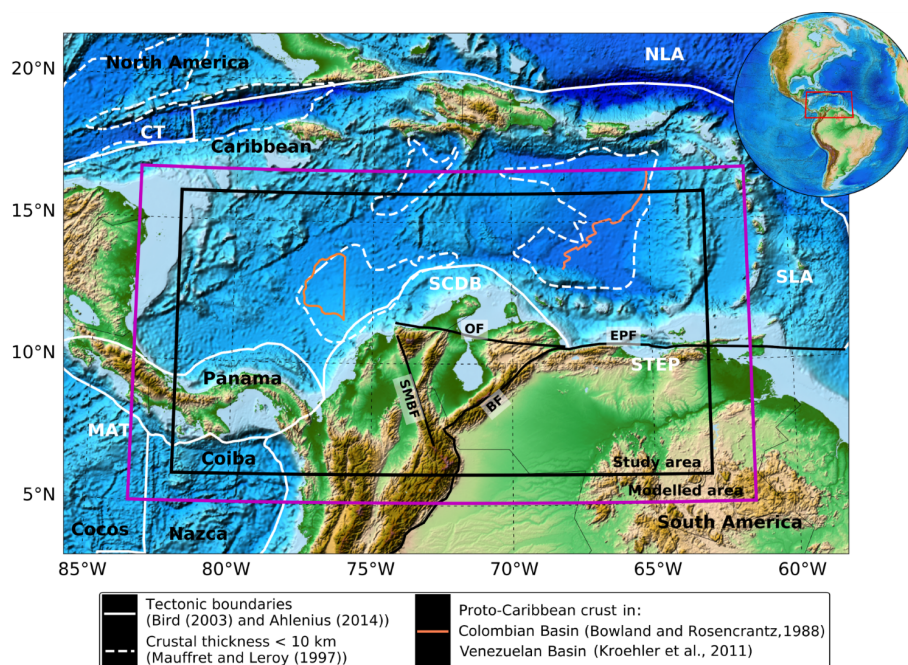


Figure 1. Location of the regions for models (magenta box) and interpretations (black box). The modelled area involves four tectonic plates: Caribbean, Panama, Nazca (Coiba microplate), and the north of South American plate. Black lines represent the main faults. BF is the Boconó Fault, CB is the Colombian Basin, CT is the Cayman Trough, EPF is the El Pilar Fault, NLA is the northern Lesser Antilles subduction, MAT is the Middle American Trench, OF is the Oca Fault, SCDB is the South Caribbean Deformed Belt, SLA is the southern Lesser Antilles subduction, SMBF is the Santa Marta-Bucaramanga Fault, STEP is the Subduction–Transform–Edge–Propagator fault system, and VB is the Venezuelan Basin. Shade relief image from Amante and Eakins (2009).

esis that the C-LIP formed above the Galápagos hotspot. However, offsets of ~ 1200 – 3000 km are obtained between the present-day Galápagos hotspot location and the plume conduits back to 90 Ma, as previously reported by Pindell et al. (2006) and Boschman et al. (2014).

2 Tectonic setting of the Caribbean and north-western South America

2.1 The Caribbean Large Igneous Plateau

The Caribbean oceanic crust is the complex product of the interaction of a mantle plume with the Proto-Caribbean (Farallon) plate 90 Ma ago, forming the second largest plateau after the Ontong Java (Kerr, 2014). Melt modelling of the high-MgO plateau lavas found in Curaçao suggest that the primary magmas contained up to 24 wt% MgO and that they correspond to a 30%–32% partial melting of a fertile, heterogeneous peridotite, with a potential temperature of 1564–1614 °C (Hastie and Kerr, 2010; Kerr, 2014).

Due to the fact that most of the plateau is currently submerged below large water depths, its structure and geochemistry has been mainly constrained from accreted material along the Caribbean margins, including Colombia, Ecuador, Costa Rica, Jamaica, and Hispaniola (Kerr, 2014; Kerr and

Tarney, 2005; Van Der Lelij et al., 2010). In summary, the accreted fragments consist of basaltic and picritic lavas and sills, with gabbros and ultramafic cumulates (Kerr, 2014).

Diebold and Driscoll (1999) and Driscoll and Diebold (1999) presented the most detailed model of the formation of the C-LIP, which they based on seismic reflection profiles. According to their model, the Proto-Caribbean crust formed in the eastern Pacific by seafloor-spreading in the Late Jurassic–Early Cretaceous. This crust had a normal thickness (~ 6 km) that later on during the pre-Senonian interacted with a mantle plume. As a result, a widespread eruption of the first basaltic flows, accompanied by extension and thinning of the Proto-Caribbean crust took place. Additionally, the intrusion of igneous material and underplating of residual mantle and ultramafic cumulates contributed to the formation of the thicker portions of the Caribbean plate, which in some places can reach up to 20 km. Following this, during the Senonian additional extension and underplating occurred, causing the uplift and rotation of the Beata Ridge, accompanied by the late stage of basaltic flows. Thus, at least two main pulses of magmatic activity have been identified: at ~ 91 – 88 and ~ 76 Ma (Diebold and Driscoll, 1999; Sinton et al., 1998).

Nowadays, it is possible to recognize anomalously thin, extended Proto-Caribbean crust, where crustal thickness

ranges between 2.8 and 5 km, in the south-eastern Venezuelan Basin and in some regions of the Colombian Basin. These thin areas are characterized by a rough basement (B'' horizon), suggesting that no basalt flows covered these domains. The Moho depth also shows a spatial variation: it shallows abruptly below the rough B'' basement and deepens in areas where the B'' horizon is smooth (Driscoll and Diebold, 1999). Figure 1 depicts the areas of thinned Proto-Caribbean crust as orange lines in the Colombian Basin (Bowland and Rosencrantz, 1988) (closed polygon) and in the Venezuelan Basin (Kroehler et al., 2011) (eastward of the orange line).

Although there is strong geochemical evidence that supports the origin of the C-LIP as melting of the paleo-Galápagos plume head (Geldmacher et al., 2003; Hastie and Kerr, 2010; Kerr and Tarney, 2005; Thompson et al., 2004), recent kinematic reconstructions back to 90 Ma by Boschman et al. (2014) showed an offset of up to 3000 km between the present-day Galápagos hotspot and the location of the Caribbean plate.

2.2 Nazca and Caribbean subductions

The northern margin of the South American plate is an active zone with two flat-slab subductions that interact at depth: the Nazca (Coiba microplate) plate from the west and the Caribbean plate from the north (some recent references include Bernal-Olaya et al., 2015; Chiarabba et al., 2015; Monsalve et al., 2019; Porritt et al., 2014; Siravo et al., 2019; Syracuse et al., 2016; Vargas and Mann, 2013; Wagner et al., 2017; Yarce et al., 2014). This complex interaction defines a poorly understood tectonic setting. Indeed, the geometry of these subductions is not well constrained yet, although different attempts have been made (e.g. Van Benthem et al., 2013; Bezada et al., 2010; Hayes et al., 2018; Mora et al., 2017).

Since the Late Cretaceous, the oblique collision of the Caribbean plate due to its east–north-east migration from the Pacific Ocean has shaped the South Caribbean margin. As a consequence, several foreland basins have been formed in the north of the South American continent, following the diachronous displacement of the collision front (Escalona and Mann, 2011 and references therein).

Along this margin, the Caribbean plate has subducted beneath the continental South American plate and the Maracaibo block since the Late Cretaceous (Kroehler et al., 2011), forming the South Caribbean Deformed Belt (SCDB; see Fig. 1). However, the lateral extension of this subduction has been actively debated. For instance, the tomographic model of Van Benthem et al. (2013) showed positive P-wave velocity anomalies from 76 to 67° W that were only traced in the upper mantle, suggesting that the subduction is ongoing along most of the margin, excluding the southwestern edges with the South American plate and the Panama microplate. According to Kroehler et al. (2011), in the southeast portion of the Caribbean plate an incipient subduction might be developing at present.

From the Pacific, the subduction of the Nazca plate shapes the western margin of the South American continent. In Colombia, north of the Caldas tear ($\sim 5^\circ$ N) the subduction becomes flat (Chiarabba et al., 2015; Vargas and Mann, 2013; Wagner et al., 2017) and is likely associated with the down-going Coiba microplate (Fig. 1). This flat-slab subduction is characterized by a buoyant oceanic crust, which Chiarabba et al. (2015) associated with a volcanic ridge.

3 Modelling approach

The first steps in the modelling workflow were to define a structural starting model and to assign the densities to the upper most lithospheric layers. Following this, different mantle density configurations were tested (Sect. S1 in the Supplement). The gravity response of these 3D lithospheric-scale structural and density models were computed with the software IGMAS+ (Schmidt et al., 2011) at 10 km calculation height. The modelled results were compared with the free-air gravity anomalies of EIGEN-6C4 (Förste et al., 2014), available at the Calculation Service of the International Centre for Global Earth Models (ICGEM; Ince et al., 2019). The modelled area is shown as a magenta box in Fig. 1 and ranges between approximately 5 and 16° N and 62 and 83° W.

In the following subsections, the datasets used to constrain the initial structural model are presented (Sect. 3.1). Additionally, because the gravity anomalies of larger wavelengths are especially sensitive to deep density contrasts, the initial density configuration took into account the evaluation of the mantle density effect in the gravity model (Sect. 3.2). Finally, Sect. 3.3 provides the details about the forward-modelling of the gravity residuals of the initial lithospheric configuration, which includes the definition of two high-density bodies in the uppermost lithospheric mantle (< 50 km). The general methodological workflow is shown in Fig. 2.

3.1 Input data

The lithospheric structural starting model includes the thicknesses of eight interfaces: (1) seawater (Fig. 3a), obtained as the difference between sea level and the General Bathymetric Chart of the Oceans (GEBCO) (Weatherall et al., 2015); (2) oceanic and (3) continental sediments (Fig. 3b and c) taken from the CRUST1.0 dataset (Laske et al., 2013); (4) oceanic and (5) continental crystalline crust (Fig. 3d and e) considering the Moho depth from the GEMMA model (Reguzoni and Sampietro, 2015); (6) the slab shapes of the Nazca (Hayes et al., 2018) and (7) Caribbean (Mora et al., 2017) flat-slab subductions (Fig. 3f); and finally (8) the lithospheric mantle, which was subdivided into seven layers using the SL2013sv S-wave velocity model (Schaeffer and Lebedev, 2013) from 50 to 200 km depth. The integration of the different datasets was made after interpolating to a homogeneous

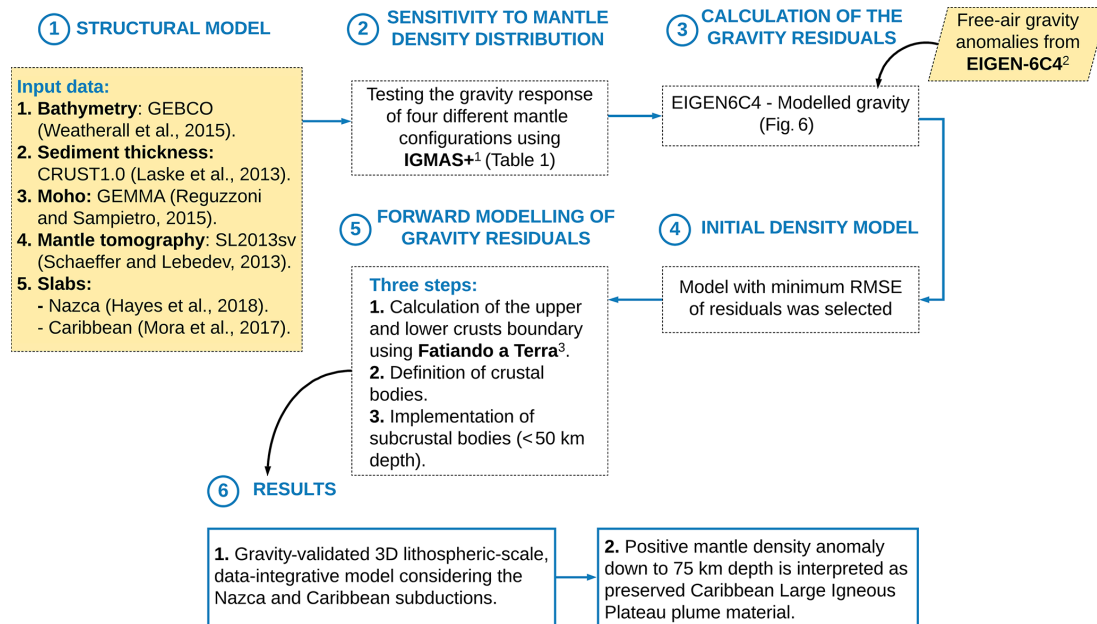


Figure 2. Methodological scheme used in this research. ¹ Schmidt et al. (2011). ² Förste et al. (2014) and Ince et al. (2019). ³ Uieda et al. (2013).

spatial resolution of 25 km, using the minimum curvature algorithm with the software Petrel (© Schlumberger Ltd).

The sediment thickness from CRUST1.0 was selected not only because it includes the continental regions but also because it takes into account information from broadly distributed seismic profiles of EXXON (1985) that allow the recognition of the main sedimentary features without disregarding the spatial connection between both inland and offshore sedimentary systems. The sea level was used as the boundary zone between the oceanic and the continental depocentres.

Additionally, the continent–ocean transition (COT) defined by Gómez-García et al. (2019a, b) was used to separate both oceanic and continental crustal types. The black dashed lines in the oceanic crust map (Fig. 3d) depict regions where the crust has a thickness smaller than 10 km according to Mauffret and Leroy (1997). Most of these regions coincide with places where the calculated crustal thickness is extremely thin, with values lower than 4 km.

Finally, even though the 3D mantle densities published by Gómez-García et al. (2019a, b) were considered (see Sect. 3.2), whose approach takes into account the mineralogical composition of the mantle and the S-wave velocities of Schaeffer and Lebedev (2013), the gravity signal of the Nazca and Caribbean slabs was also tested. The Nazca subduction was taken from the Slab2 dataset (Hayes et al., 2018), which integrates diverse geophysical information into the definition of the slab’s 3D structure, including active-source seismic data, receiver functions, seismicity catalogues from local and regional networks, and tomographic models.

On the other hand, the Caribbean slab was defined following the hypocentral distribution (Mora et al., 2017). Figure 3f presents the integrated thickness of both flat slabs. In the region where both subducting plates interact at depth the integrated thickness reaches more than 120 km. While the Slab2 dataset includes the Nazca slab thickness, in the Caribbean case a thickness of ~ 70 km was assumed a priori (see Fig. S2 in the Supplement).

3.2 Initial lithospheric configuration and the mantle density effect on the gravity signal

The lithospheric mantle density is one of the most influential parameters in the modelling of the gravity anomalies because of its massive volume compared to the other lithospheric layers. The mantle density effect on the gravity signal was explored by testing four different mantle configurations (see Sect. S1). The model with the minimum RMSE compared with EIGEN-6C4 was selected as the initial lithospheric configuration. This model includes the 3D mantle densities obtained from the conversion of the S-wave velocity anomalies of the SL2013sv model (Schaeffer and Lebedev, 2013), from 50 to 200 km depth, published by Gómez-García et al. (2019a, b). In this approach, the density conversion is performed following a modified version of Goes et al. (2000) method, using a pressure- and temperature-dependent expansion coefficient (Hacker and Abers, 2004; Meeßen, 2017).

Figures S3 and S4 present the S-wave velocities at different depths (from 50 to 200 km, every 25 km) and their associated densities, respectively. In general, with this approach it is possible to establish a relation between high-velocity

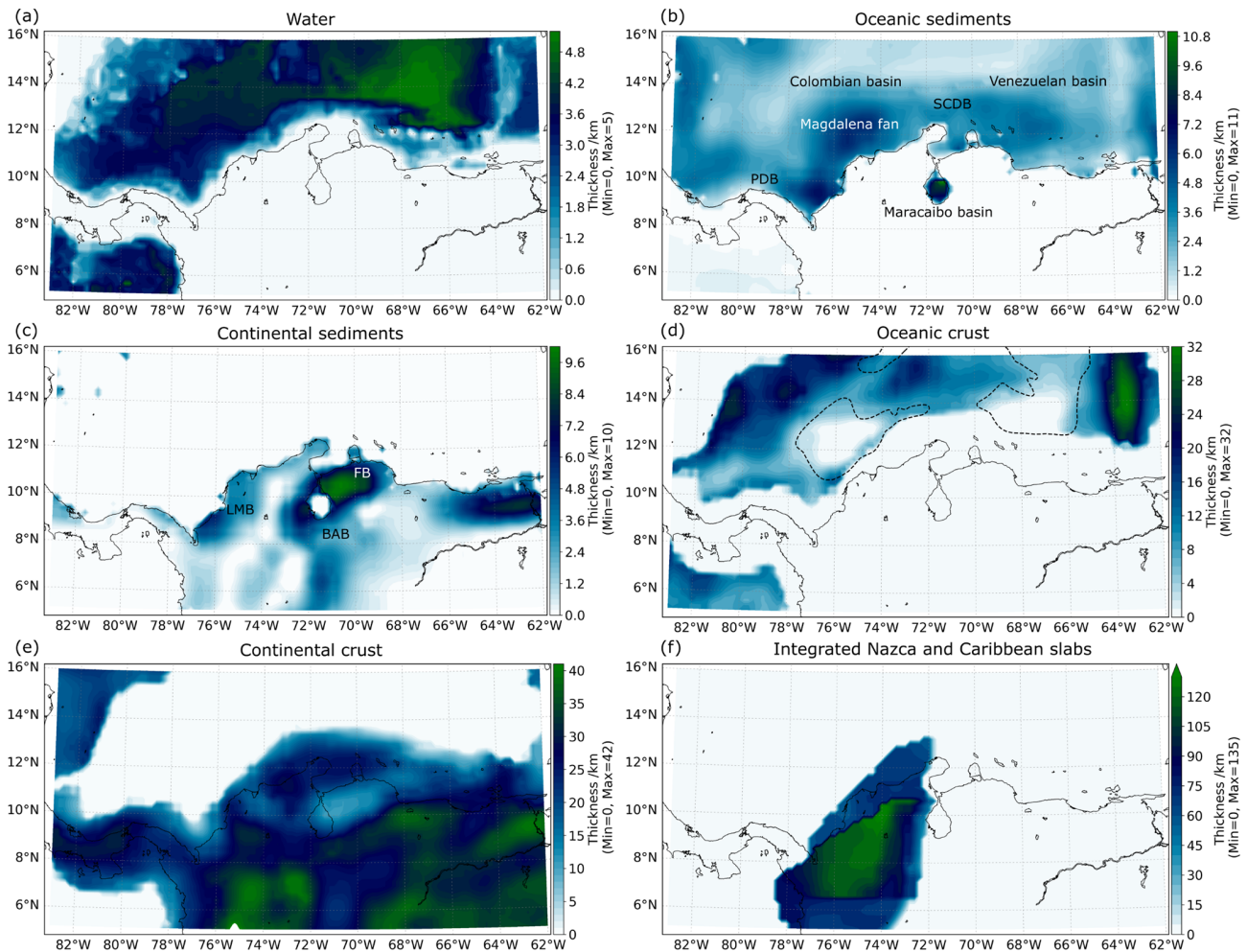


Figure 3. Structural layers used in the starting model: (a) water thickness from GEBCO (Weatherall et al., 2015), (b, c) unconsolidated oceanic and continental sediments based on CRUST1.0 (Laske et al., 2013), (d, e) oceanic and continental crystalline crust thicknesses (the dashed lines in d represent places where the oceanic crust is thinner than 10 km; Mauffret and Leroy, 1997); (f) integrated slab thickness from the Nazca (Hayes et al., 2018) and Caribbean (Mora et al., 2017) subductions. The independent thickness maps of the slabs are presented in Fig. S2. BAB is the Barinas-Apure basin. FB is the Falcón Basin. LMB is the Lower Magdalena Basin. PDB is the Panamá Deformed Belt. SCDB is the South Caribbean Deformed Belt.

anomalies and high mantle densities (blue and dark blue regions in Fig. S3 and S4, respectively) and vice versa with low velocities and low mantle densities. Figure 4 summarizes the conversion results as described hereafter.

The mantle structure shows two different trends. At depths shallower than 75 km, in the Caribbean Sea the mantle is denser compared with the one below the South American continent, with differences up to 40 kg m^{-3} at 50 km depth. Although the mantle density increases with depth, it is possible to distinguish a subduction-like behaviour from 125 to 200 km below the surface: denser (colder) material below the South American continent, in contrast with a lighter (warmer) mantle below the ocean. These two trends are summarized in Fig. 4a and c for depths shallower than 75 km and in Fig. 4b and d for those deeper than 125 km depth.

Based on the spatial distribution of both parameters (velocity and density), it is not easy to differentiate which portions of the mantle belong to either the Caribbean or the Nazca slabs. Nevertheless, the fastest velocities (up to 4580 m s^{-1}) are concentrated between 68 and 77° W , from 125 down to 200 km depth (Figs. 4b and S3).

Because at depths shallower than 125 km the observed patterns do not allow us to make a reliable interpretation about the slabs, it was necessary to explore the gravity effect of both subducting slabs using additional datasets. Figure 5a shows the spatial distribution of the depth to the top of the Nazca (Coiba) slab, as published by Hayes et al. (2018). Two main factors can be highlighted from this geometry: (1) even though it has been published as the Nazca subduction, it is very likely that it also includes an important fraction of the Caribbean slab because of its northward exten-

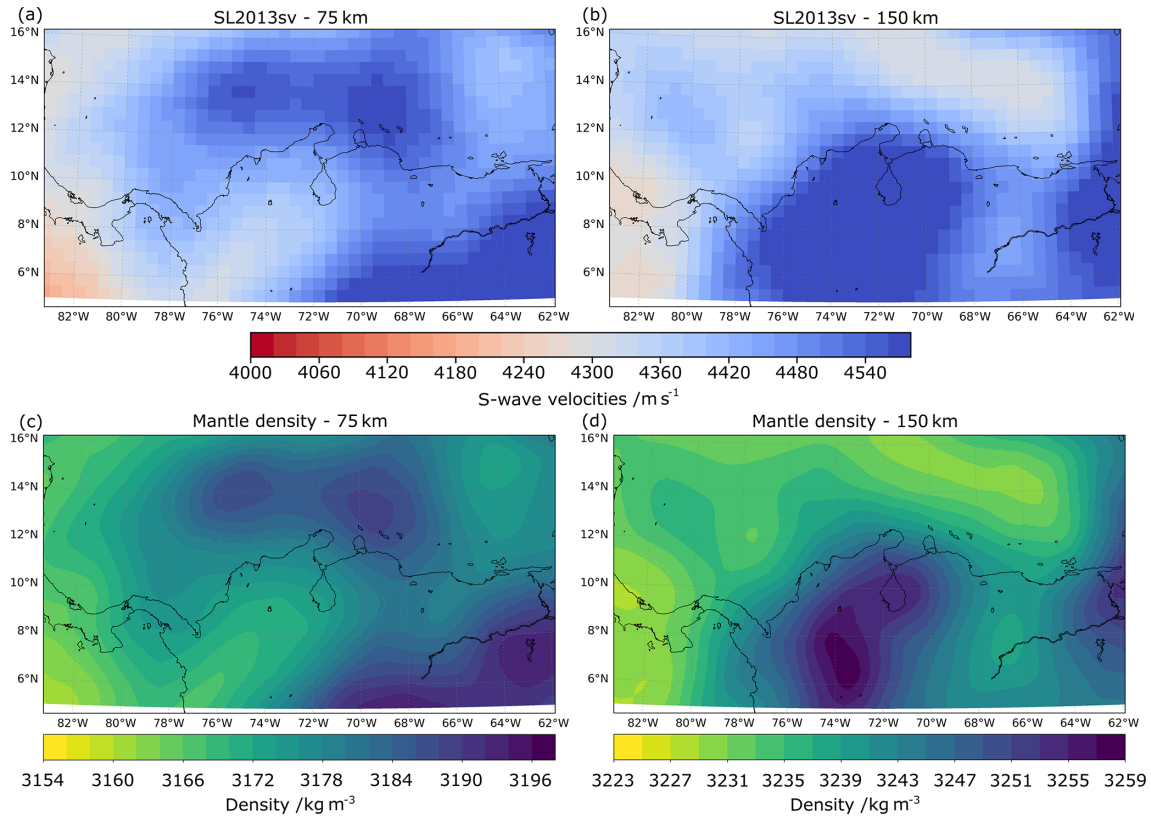


Figure 4. Relation between the S-wave velocities from the SL2013sv model (Schaeffer and Lebedev, 2013) and the calculated mantle densities. (a, b) S-wave velocities at 75 and 150 km depth, respectively. The original cell size of the tomographic data is $0.5^\circ \times 0.5^\circ$. (c, d) Corresponding densities at 75 and 150 km depth following Goes et al. (2000) and Meeßen (2017) (see the text for details of the conversion). In this case the S-wave velocities were interpolated to a spatial resolution of 25 km to make them consistent with the spatial resolution of the rest of the lithospheric layers.

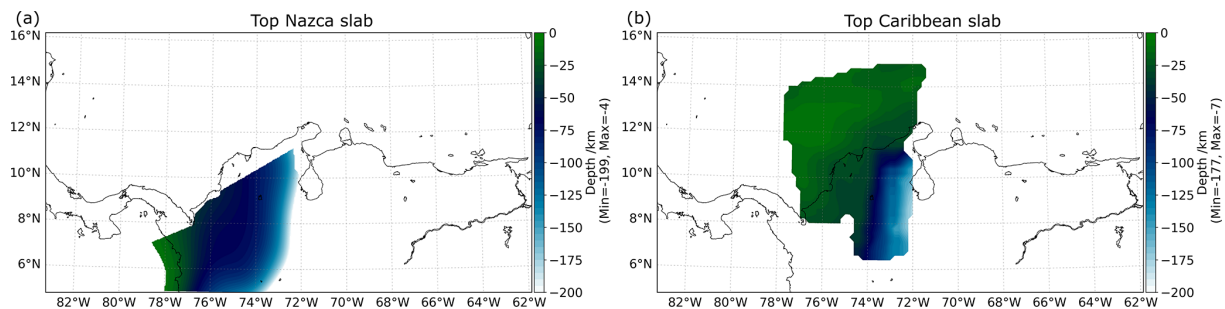


Figure 5. Depth to the top of the slabs tested in the lithospheric-scale gravity models. (a) Nazca geometry from the Slab2 dataset (Hayes et al., 2018). Note that this geometry does not differentiate the Nazca (Coiba) and the Caribbean components in the slab. (b) Caribbean slab as published by Mora et al. (2017).

sion, and (2) it is possible to distinguish its flat shape, which widens towards the east, in the region north of the Caldas tear ($\sim 5^\circ$ N), as previously reported by other authors (e.g. Chiarabba et al., 2015; Vargas and Mann, 2013). Similarly, Fig. 5b depicts the depth to the top of the Caribbean slab by Mora et al. (2017), which according to these authors is present westward of $\sim 72^\circ$ W. This geometry suggests that

the Caribbean subduction is not entirely flat, but a sharp increase in its angle is present towards the south and south-east.

Table 1 summarizes the densities assumed in the initial 3D lithospheric model for the different layers considered. This model includes the gravity response of the 3D mantle densities in addition to the integration of the Nazca and Caribbean slabs geometries, as represented in Fig. 3f. When both slabs are integrated into the model, a density of 3163 kg m^{-3} is ob-

Table 1. Summary of the datasets used to constrain the initial 3D lithospheric-scale model of the South Caribbean and north-western South American plate and the density values (kg m^{-3}) assumed for each layer.

Layer	Density	Reference of structural layer
Water	1040	GEBCO (Weatherall et al., 2015)
Oceanic sediments	2350	CRUST1.0 (Laske et al., 2013)
Continental sediment	2500	CRUST1.0 (Laske et al., 2013)
Oceanic crust	2900	Moho depth from GEMMA model
Continental crust	2800	Reguzzoni and Sampietro (2015)
Nazca slab	3163	Slab2 (Hayes et al., 2018)
Caribbean slab	3163	(Mora et al., 2017)
Mantle from Moho down to 50 km depth	3200	–
Mantle from 50 down to 200 km depth	3D density solution	SL2013sv tomographic model (Schaeffer and Lebedev, 2013)

tained with the IGMAS+ inversion algorithm (Sæther, 1997; Schmidt et al., 2011).

3.3 Forward-modelling of the gravity residuals

After the analysis of the mantle density effect on the modelled gravity was performed, the model which had the minimum RMSE compared with the observed gravity anomalies of the EIGEN-6C4 dataset (Förste et al., 2014) was selected as the initial lithospheric configuration (Sect. 3.2).

The relatively short wavelengths of the still-remaining gravity residuals (observed gravity minus modelled gravity) associated to this model account for rather shallow density heterogeneities. Indeed, the initial model considered the oceanic and continental crusts as homogeneous layers with constant densities (see Table 1). Therefore, in order to have a better representation of the crustal heterogeneities, the forward-modelling of the gravity residuals of the initial model was performed in three main steps. First, the code “Harvester” of the Fatiando a Terra geophysical Python tool (Uieda et al., 2013) was used for defining the boundary between the upper and lower continental and oceanic crusts. Harvester plants “density seeds” at the base of the crust and makes them grow vertically until the gravity residuals are minimized, defining the top of the lower crust. In our case, a density contrast of 300 kg m^{-3} was assumed between the upper and lower crust for this inversion.

Second, in the regions where the residuals (after the inversion with Harvester) were still considerably large (> 30 and $< -30 \text{ mGal}$), bodies in the upper and lower crust within the oceanic and continental domains were defined (see Sect. 4.1). The delimitation of these bodies took into account the geologic evolution of the C-LIP and the tectonics of the Caribbean provinces in general (e.g. well-known volcanic arcs, previously reported underplated material, or extended proto-Caribbean crustal domains). Their densities were assigned depending on whether they matched a positive or negative residual, which suggest a mass deficit or excess in the initial model, respectively.

Finally, after implementing the previously mentioned two steps, large gravity residuals of medium-size wavelengths were still present in the oceanic domain of the Caribbean, which led us to define two high-density bodies in the uppermost oceanic lithospheric mantle ($< 50 \text{ km}$) of the Colombian and the Venezuelan basins. At shallow depths, trade-offs between the crust and the shallow mantle may occur, affecting the reliability of the tomographic data.

4 Results

After testing the gravity response to different mantle configurations, the model that integrates all the regional scale observations was selected as the initial lithospheric configuration (Table 1). The residuals associated with this model are depicted in Fig. 6 and have an RMSE of 28.84 mGal , the minimum value of all tested models (Sect. S1). The wavelength of these residuals indicates that they are mainly due to shallow heterogeneities that were not considered in the initial set up of the model. Therefore, the forward-modelling of these residuals was used to derive density heterogeneities on a regional scale that are present within the continental and oceanic crystalline crusts and in the uppermost ($< 50 \text{ km}$ depth) lithospheric mantle, as described in the following subsections.

4.1 Crustal structure of the Caribbean and north-western South American plates

Figure 7a depicts the observed free-air gravity of EIGEN-6C4 at 10 km calculation height. This field has large positive values ($> 180 \text{ mGal}$) over the topographic highs of the Andes, as well as over the Santa Marta massif and the Panama microplate (Fig. 1). In contrast, negative gravity anomalies lie over the thick depocentres of the South Caribbean margin (Panama Deformed Belt, Magdalena Fan, and South Caribbean Deformed Belt; Fig. 3b), as well as over most of the continental basins (Lower Magdalena, Barinas-Apure, and Maracaibo; Fig. 3b, c).

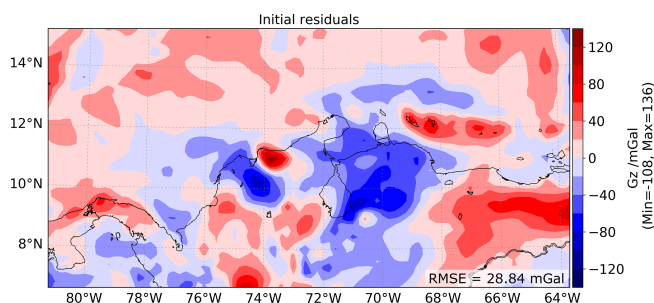


Figure 6. Gravity residuals of the initial lithospheric configuration, assuming the densities in Table 1. Here, large misfits with a dominance of short (few kilometres) and medium (hundreds of kilometres) wavelengths suggest density heterogeneities in the shallower domains of the lithosphere that were not considered in the initial set-up of the model.

Table 2. Summary of the layers and density values that integrate the final structural model of the South Caribbean and north-western South American lithosphere.

Layer	Modelled density (kg m^{-3})
Water	1040
Oceanic sediments	2350
Continental sediments	2500
Oceanic upper crust	3000
Low-density upper crustal body (Aves Ridge)	2900
High-density upper crustal body (Venezuelan Basin)	3300
Oceanic lower crust	3100
Low-density lower crustal bodies (Aves Ridge and South Nicaraguan Rise)	3000
High-density lower crustal bodies (Colombian and Venezuelan basins)	3250
Continental upper crust	2750
Low-density bodies upper continental crust (eastern cordillera and Lower Magdalena Basin)	2600–2650
High-density body upper continental crust (Santa Marta Massif)	3000
Continental lower crust	3070
High-density subcrustal bodies down to 50 km depth	3242
Mantle down to 50 km	3200
Nazca and Caribbean slabs	3163
Mantle from 50 to 200 km	3D density solution

As described in Sect. 3.3 the first two steps of the forward-modelling process consisted of including crustal heterogeneities that aim to fit the gravity field. Figure 7b shows the residuals associated to a model in which the gravity signal of the water, sediments, heterogeneous crystalline crust, and mantle (deeper than 50 km) were considered. Here, two positive anomalies remain in the Colombian and Venezuelan basins. Thus, the third step on the forward-modelling required the addition of two subcrustal bodies to compensate the gravity misfit in these domains. These bodies are located between the Moho and 50 km depth and have an average density of 3242 kg m^{-3} .

As can be seen in Fig. 7c, after forward-modelling the gravity residuals including the subcrustal bodies, the modelled gravity response resembles the features previously described for the EIGEN-6C4 field. The new residuals have an RMSE of 17.45 mGal and have been minimized for the entire study area (Figs. 7d and S5f) compared with the residuals of the initial model (Figs. 6 and S5d). With the new lithospheric configuration, a decrease of approximately 39.5 % in the RMSE is reached.

This new lithospheric configuration aims to represent the complex tectonic setting of the Caribbean crust by including six different oceanic layers, with low- and high-density bodies (Fig. 8) as summarized in Table 2. The oceanic upper crust has been modelled with an average density of 3000 kg m^{-3} and its maximum thickness reaches up to 9.55 km (Fig. 8a). Moreover, low- and high-density bodies were defined within this layer. A low-density domain is present below the Aves Ridge (yellow polygon), with an average density of 2900 kg m^{-3} , while a high-density body was found below the Venezuelan Basin (magenta polygon), whose average density is 3300 kg m^{-3} .

The oceanic lower crust (Fig. 8b) has been modelled with an average density of 3100 kg m^{-3} . Within this layer, widely distributed high-density bodies are required to fit the gravity field both for the Colombian and the Venezuelan basins (magenta polygons), with an average density of 3250 kg m^{-3} . The density assigned to the low-density bodies located in the Aves Ridge and the South Nicaraguan Rise is 3000 kg m^{-3} . The maximum thickness of this layer is 24.7 km, towards the west of the Aves Ridge.

As a reference, Fig. 8a includes the places where Mauffret and Leroy (1997) reported a thinner oceanic crust ($< 10 \text{ km}$, dashed black lines). Similarly, Fig. 8b depicts the areas where extended Proto-Caribbean crust has been reported in the Colombian and the Venezuelan basins (black lines, numbers 1 and 2). Note the relation between these extended domains and the thin ($< 1 \text{ km}$) or almost non-existent crust present in the structural model.

The continental crust has been split into four different sub-layers. The continental upper crust (Fig. 8c) has the maximum thickness (up to 35.3 km) and an average density of 2750 kg m^{-3} . Two low-density bodies were defined within this layer in order to improve the gravity fit. These areas include parts of the Lower Magdalena, Maracaibo, and Falcon basins (yellow polygons). Such bodies have an average density of $2600\text{--}2650 \text{ kg m}^{-3}$. Additionally, one high-density body has been integrated into the structure of the upper continental crust (magenta polygon). It has been modelled with an average density of 3000 kg m^{-3} and is located below the Santa Marta massif, bounded by the Oca and the Santa Marta-Bucaramanga faults.

Finally, the lower continental crust has been defined as a complete unit, with an average density of 3070 kg m^{-3} and a maximum thickness of 31.8 km reached in the southern part of the eastern cordillera.

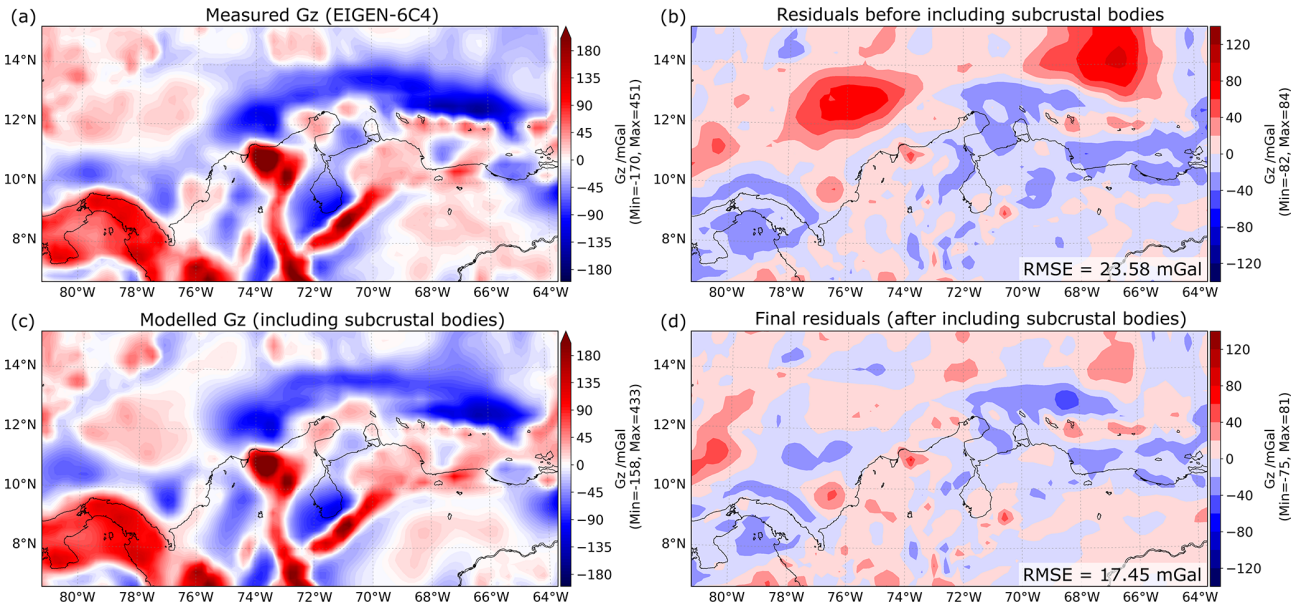


Figure 7. Gravity anomalies (Gz) with (a) measurements available in the EIGEN-6C4 dataset at 10 km height (Förste et al., 2014; Ince et al., 2019). (b) Residuals of a model in which the subcrustal bodies are not included. (c) Gz after forward-modelling the gravity residuals of the initial lithospheric configuration. The modelling included the definition of crustal and subcrustal bodies (see the text for details). (d) Final residuals obtained with the lithospheric structure described in Table 2.

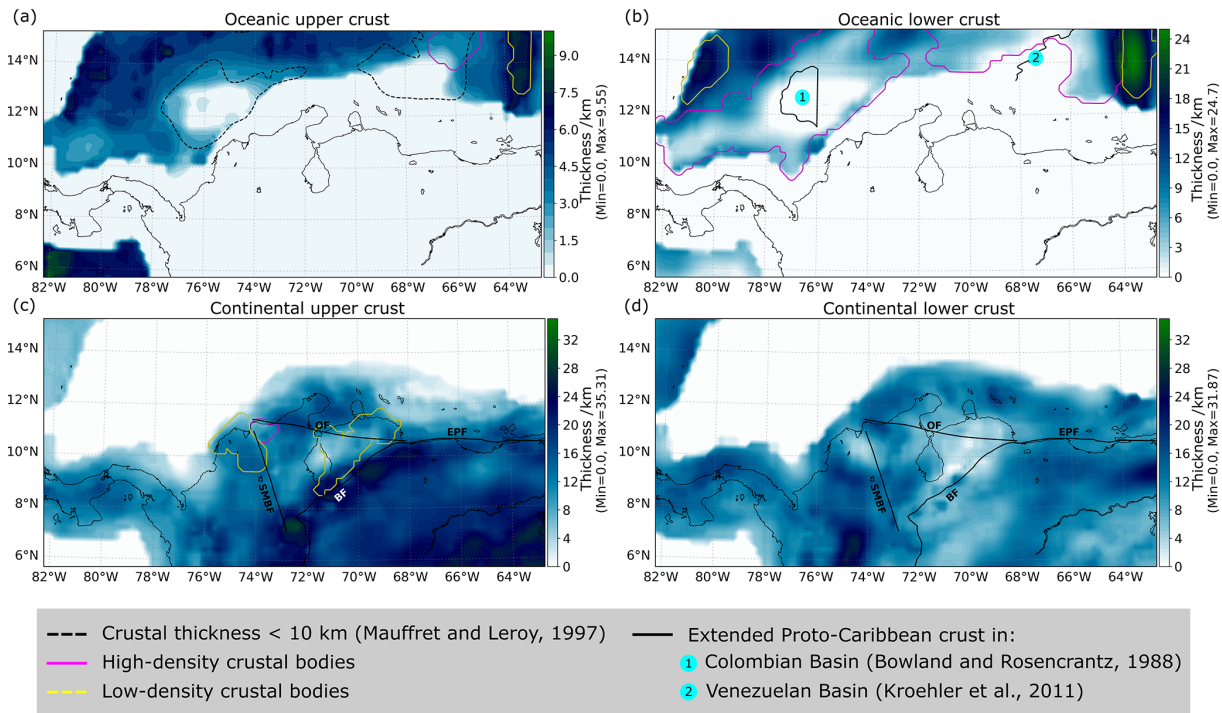


Figure 8. Thickness of the (a) oceanic upper crust, (b) oceanic lower crust, (c) continental upper crust, and (d) continental lower crust. Dashed polygons in (a) represent places where the oceanic crust is thinner than 10 km (Mauffret and Leroy, 1997). Black polygons in (b) depict areas with smooth basement (B'' horizon), associated with extended Proto-Caribbean crust in the Colombian Basin (Bowland and Rosencrantz, 1988) (number 1) and in the Venezuelan Basin (Kroehler et al., 2011) (eastward of the black line, number 2). Main continental faults are shown as thick black lines in (c) and (d). The final lithospheric model includes different high- and low-density bodies in the oceanic and continental crusts, depicted as magenta and yellow polygons, respectively. Acronyms are the same as in Fig. 1.

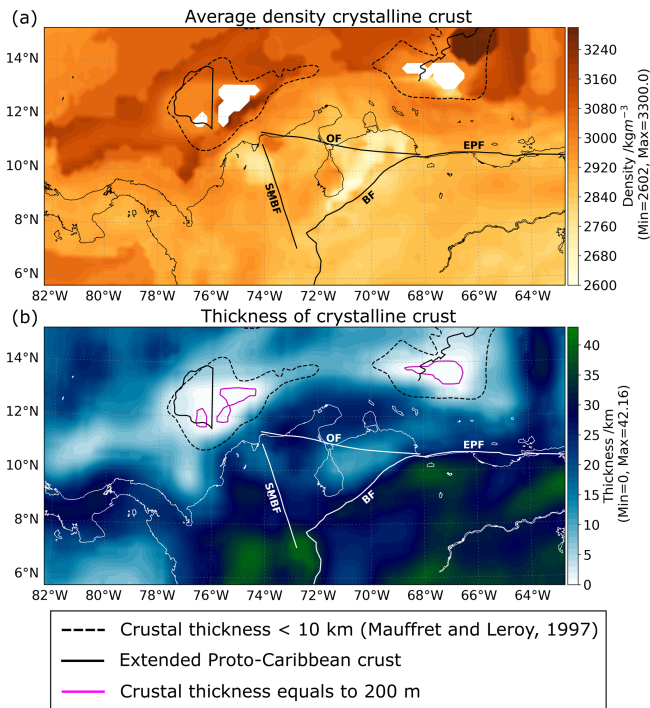


Figure 9. The average density of the crystalline crust obtained after forward-modelling the gravity residuals highlights areas where the high-density material of the C-LIP formation strongly affected the Proto-Caribbean crust. (a) Average density of the South Caribbean and north-western South American crusts based on the forward-modelling of the gravity residuals. The crustal domains summarized in Table 2 have been included. White domains represent areas where the thickness of the oceanic crust is virtually zero, according to the integrated datasets. (b) Thickness of the crystalline crust used in the data-integrative 3D model (see Sect. 3.1). Magenta polygons are contours of 200 m thickness. Other polygons as depicted in Fig. 10. Acronyms are the same as in Fig. 1.

Assuming this new lithospheric configuration, the average crustal density highlights high- and low-density domains that correspond with thin and thick crystalline crust, respectively (Fig. 9). In general, it is possible to recognize that lighter crust (Fig. 9a) is associated with the continental domains, as well as with portions of the oceanic arc-like Nicaraguan Rise (Lewis et al., 2011), and the extinct arc of the Aves Ridge (Christeson et al., 2008). On the other hand, the highest densities are concentrated in the Colombian and the Venezuelan basins. Two regions where the calculated thickness of the oceanic crust is “virtually zero” are depicted as white areas in Fig. 9a and as magenta polygons in Fig. 9b and will be discussed in Sect. 5.2.

Within the continental domain, two low-density regions ($< 2700 \text{ kg m}^{-3}$) are inferred based on the model results: the Lower Magdalena Valley Basin, whose basement has been described as mainly felsic (Mora-Bohórquez et al., 2017), as well as parts of the Falcon and Maracaibo foreland basins. These continental basins are characterized by

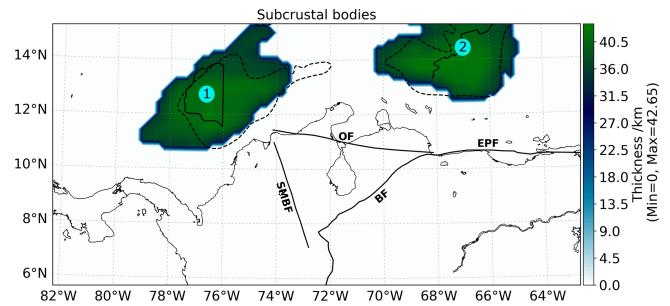


Figure 10. Two high-density subcrustal bodies are required to fit the gravity field. These bodies have a spatial correlation with the thin crust in the Colombian and the Venezuelan basins. Polygons are as described in Fig. 8. Acronyms are the same as in Fig. 1.

a thin crust ranging between ~ 10 and 20 km (Fig. 9b). In contrast, the crust of the Santa Marta massif has an average density of $\sim 3000 \text{ kg m}^{-3}$, which is in agreement with a cratonic origin with igneous intrusions, as described by Montes et al. (2019a).

4.2 Oceanic upper mantle structures

In order to fit the gravity, two subcrustal bodies were additionally required and integrated into the oceanic upper mantle ($< 50 \text{ km}$ depth) (Fig. 10). According to the model results, these bodies might reach an average density of $\sim 3300 \text{ kg m}^{-3}$ if they are placed from the Moho down to 25 km depth (see Fig. S6). Alternatively, an average density of 3242 kg m^{-3} is required if they extend down to 50 km depth. Due to the fact that a similar high-velocity trend – that would convert to comparable densities – can be followed in the tomographic data integrated into the lithospheric model, down to 75 km depth, the last scenario is selected hereafter as the final lithospheric configuration. These high-density bodies spatially correlate with the areas of thin crust according to Mauffret and Leroy (1997) (dashed lines in Fig. 10) but also include the regions where original Proto-Caribbean crust has been identified by Bowland and Rosencrantz (1988) in the Colombian Basin and by Kroehler et al. (2011) in the Venezuelan Basin (black lines in Fig. 10 – number 1 and 2, respectively). Thus, the high-density bodies are placed in areas where the already shallow crust–mantle boundary is insufficient to account for the excess mass needed to fit the observed gravity.

A summary of the final lithospheric structural and density model is presented in Table 2. As mentioned in Sect. 3.3, the gravity inversion was focused on improving the structural resolution for the oceanic and continental crust and the uppermost oceanic mantle; therefore, the remaining lithospheric layers were preserved as in the initial (reference) model.

5 Discussion

The gravity response of a 3D lithospheric-scale model of the Caribbean and northern South American plates – including up-to-date geophysical information – provides additional constraints regarding density heterogeneities in the lithosphere. Although a heterogeneous crust was integrated into the model in order to reduce the misfits between modelled and observed gravity, two large positive residuals in the oceanic domain (Fig. 7b) suggest additional density heterogeneities in the oceanic upper mantle (< 50 km depth), which was initially modelled with a constant density. Our approach indicates that the results of the gravity inversion are beyond the non-uniqueness of gravity because (1) the (heterogeneous) crustal densities cannot be further increased, (2) a sensitivity analysis to different mantle distributions was initially performed (Sect. S1), and (3) a high-density trend is also evidenced in the tomographic data down to 75 km depth in the Caribbean region.

In the following subsections, the implications of the high-density upper-mantle bodies are discussed, as possible plume conduits of the C-LIP currently preserved in the Caribbean upper mantle (Sect. 5.1). Additionally, different kinematic reconstructions back to 90 Ma were explored to evaluate the hypothesis that the C-LIP formed above the Galápagos hotspot. Remaining implications of the general crustal configuration are tackled in Sect. 5.2.

5.1 High-density mantle trend: preserved material of the C-LIP plume?

In the Caribbean oceanic upper mantle, two high-velocity (and therefore high-density) domains can be followed, at least down to 75 km depth, according to the S-wave tomographic model of Schaeffer and Lebedev (2013) (Figs. 4, S3 and S4) that has been integrated in the initial (reference) density model of the Caribbean. After forward-modelling the gravity residuals to identify density heterogeneities in the crystalline crust, the residuals were still large enough to call for density variations on the uppermost oceanic mantle (< 50 km depth), which was initially modelled with a constant density of 3200 kg m^{-3} (Table 1). Accordingly, the results suggest that two subcrustal bodies with positive density anomalies are present from the Moho down to 50 km depth. These bodies spatially correspond with a fast velocity mantle trend observed in the tomographic data (Fig. 11).

Assuming the thickness and spatial distribution shown in Fig. 10, an average density of $\sim 3242 \text{ kg m}^{-3}$ is required to fit the gravity field. These bodies, approximately 440 km wide, show a strong spatial correlation with the thinner crust of Mauffret and Leroy (1997) (dashed black polygons) and also with the stretched original Proto-Caribbean crust reported by Bowland and Rosencrantz (1988) in the Colombian Basin (number 1) and by Kroehler et al. (2011) in the Venezuelan Basin (eastward of the black line, number 2).

Nevertheless, it is necessary to point out that the density of these subcrustal domains might not necessarily be exactly 3242 kg m^{-3} . In fact, if their vertical extension is assumed from the Moho down to 25 km depth, the density required to fit the gravity increases to 3300 kg m^{-3} , resulting in similar gravity residuals (see Fig. S6) to the ones shown in Fig. 7d. This illustrates the range of non-uniqueness inherent to gravity modelling but also clearly demonstrates that the need for an excess of mass in these domains is robust.

In both scenarios, the subcrustal bodies might have seismic velocities similar to that of a normal mantle, making their interpretation as mantle plume-related bodies difficult, especially in the context of early seismic experiments carried out in the past. For example, Mauffret and Leroy (1997) interpreted seismic velocities of 8.1 km s^{-1} as normal mantle velocities, based on isolated sonobuoy measurements both in the Colombian and the Venezuelan basins (see Fig. 22a in their publication).

The presence of shallow subcrustal bodies has been identified for different plateaus and regions where plume interaction with old crust is inferred (see McNutt and Caress, 2007). Some examples include a 4 km thick and 200 km wide subcrustal body found in the Hawaiian–Emperor seamount chain by Watts et al. (1985). According to their interpretation, this body has unusually high seismic velocities for a normal lower oceanic crust, ranging between 7.4 and 7.8 km s^{-1} . More recently, Deng et al. (2014) reconstructed a preserved, lithospheric-scale magmatic intrusion associated with the evolution of the Emeishan Large Igneous Province down to 120 km depth.

In the Caribbean region, underplated material associated with picritic and ultramafic cumulates with seismic velocities of up to 8 km s^{-1} have been previously identified (e.g. Driscoll and Diebold, 1999; Mauffret and Leroy, 1997). However, the high-density (and thus high-velocity) material as represented in Fig. 11 was never mapped before with such detail and to points so deep beneath the Colombian and Venezuela basins. In the presence of a mantle plume, intrusion of high-density material on the overriding plate is expected. When the plume ceases, the new lithospheric system starts to cool down, and therefore high-density bodies can “freeze” (François et al., 2018) and become part of the mobile lithosphere that moves over the hot asthenospheric mantle, as expected by the plate tectonics theory. Therefore, we interpret these subcrustal bodies as preserved magmatic plume material responsible for the C-LIP formation.

Figure 11 shows a 3D perspective view of the preserved plume material assuming an S-wave velocity of 4540 m s^{-1} as the boundary of the high-density domains. The velocity contours at depths of 25, 50, and 75 km were taken as main constraints, and the form of the body in between was obtained by morphing of these contours following Brunet (2020) and Brunet and Sills (2015). A total volume of $\sim 12 \times 10^6 \text{ km}^3$ is calculated for what is interpreted as the C-LIP fossil plume conduits. Figure S7 shows the vertical relation

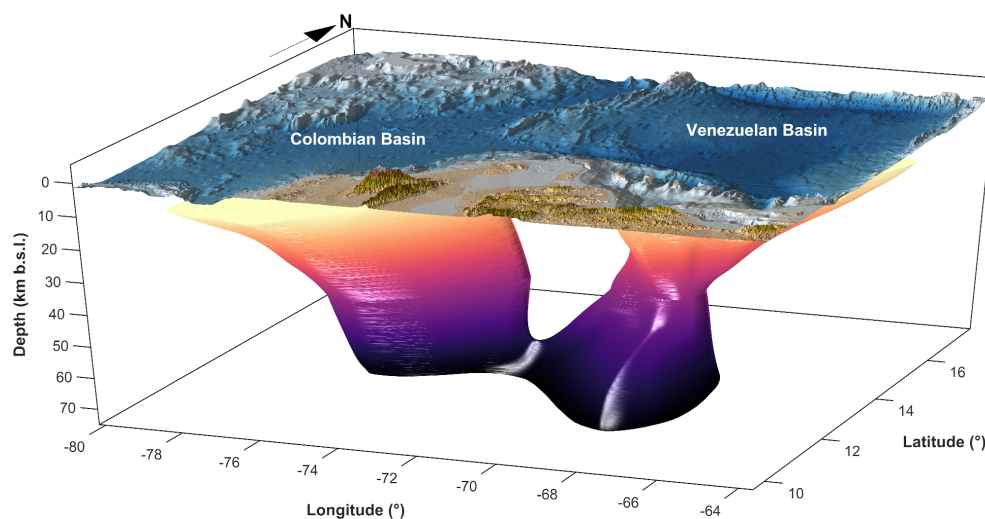


Figure 11. A 3D visualization of the interpreted preserved plume conduits, assuming an S-wave velocity of 4540 ms^{-1} as the boundary of the high-density material.

between the subcrustal bodies (if a density of 3242 kg m^{-3} is assumed for them) and the high-density trend at each depth of the tomographic model. The presence of this high-density trend down to 75 km depth suggests that it travelled with the mobile Caribbean lithosphere. Accordingly, Blanco et al. (2017) reported the lithosphere–asthenosphere boundary in the Caribbean region around 75–80 km depth.

Recently, Civiero et al. (2019) used Rayleigh–Taylor models to simulate the 3D mantle convection for Newtonian and non-Newtonian rheologies. Their results predict the development of plumelets in different stages of evolution, creating a complex structure that is sometimes difficult to image using seismic waves. Thus, the observed positive density anomalies in the Caribbean lithospheric mantle might be related with the fossil plume conduits of these type of Rayleigh–Taylor-style instabilities, similar to the ones observed in the northern East African Rift by Civiero et al. (2019).

5.2 Kinematic reconstructions of the Caribbean plateau and origin of the C-LIP

Previous studies based on geochemical analyses of C-LIP-related magmatic rocks have proposed the present-day Galápagos hotspot as the origin of the thermal anomaly responsible for the development of the C-LIP (e.g. Duncan and Hargraves, 1984; Geldmacher et al., 2003; Kerr and Tarney, 2005; Pindell and Barrett, 1990; Thompson et al., 2004). From a kinematic perspective, Nerlich et al. (2014) obtained a good fit between the paleo-position of the Caribbean plate and the present-day position of the Galápagos hotspot at the time of plateau formation (ca. 90 Ma). In their approach, the Caribbean plateau is assumed to have detached from the Farallon plate and to be fixed relative to South America at 54.5 Ma (“docking” age), while using the finite-rotation

poles from Doubrovine et al. (2012) (global moving reference model) for the motion of the Pacific and African plates. However, shortly afterwards Boschman et al. (2014) published an updated kinematic reconstruction of the Caribbean region based on an extensive compilation of geological data from the entire region, which shows a very different motion path of the Caribbean plateau relative to South America (cyan line in Fig. 12) than the model of Nerlich et al. (2014) (green line). A clear offset of the plateau to the east of the modern Galápagos hotspot at the time of C-LIP formation (90 Ma) is observed in the model of Boschman et al. (2014), as previously reported by other authors (e.g. Pindell et al., 2006). More recently, Montes et al. (2019a) reconstructed the tectonic evolution of the northern Andes–Caribbean margin and showed similar results to Boschman et al. (2014) (magenta line in Fig. 12), although a considerable difference in motion and rotation of the C-LIP between 90 and 60 Ma is evident. This difference is due to the fact the Montes et al. (2019a) reconstructions are based on tectonic units in Panama and north-western Andes terrains, while the Caribbean plate moves, bends, and deforms internally to fit those inland proxies.

Most importantly, the absolute motion of the lithospheric plates relative to the Earth’s deep interior is crucial to assess whether the C-LIP formed above the Galápagos hotspot 90 Ma ago or not. Several absolute reference models have been proposed over the last few decades, e.g. the moving Indian–Atlantic hotspots model (O’Neill et al., 2005), the fixed Pacific hotspots model (e.g. Wessel and Kroenke, 2008), the true polar wander-corrected paleomagnetic model (Steinberger and Torsvik, 2008), the subduction reference frame linking surface plate motions to subducted slab remnants mapped from seismic tomography (Van Der Meer et al., 2010), and the global hotspot moving model

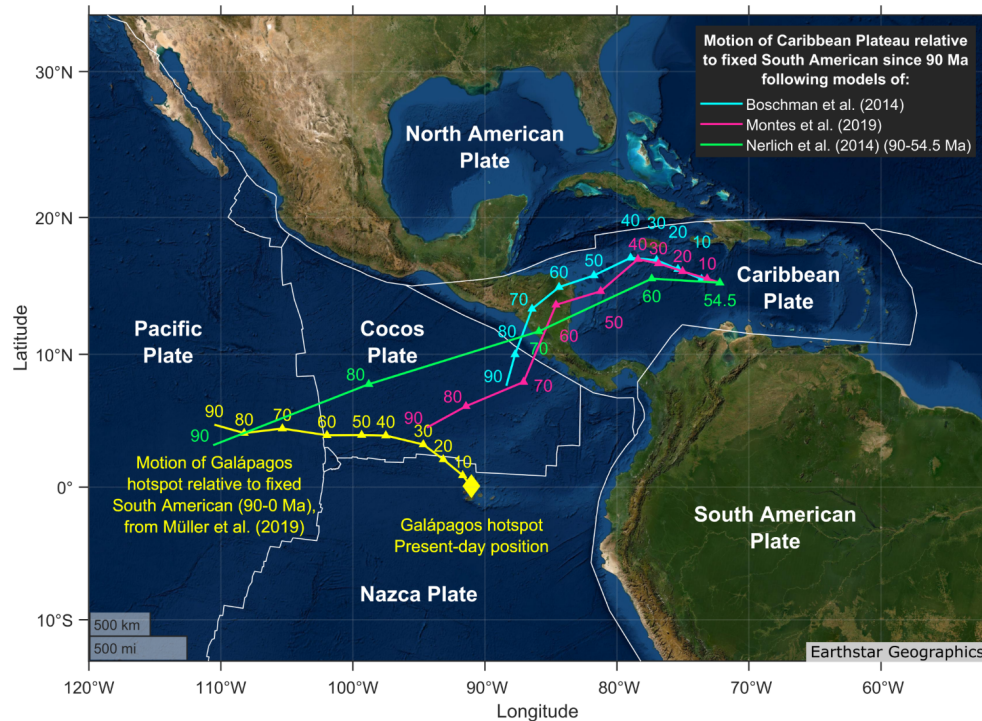


Figure 12. Motion paths of the Caribbean plate relative to the South American plate (SAM) for three recently proposed reconstructions. Motion of present-day Galápagos hotspot relative to a fixed SAM is shown in yellow. A fit with Galápagos hotspot at time of plateau formation (90 Ma) is only obtained by Nerlich et al. (2014), assuming the Caribbean plate moving with Farallon plate from 90 to 54.5 Ma and fixed to SAM since 54.5 Ma. Regional reconstructions based on geological and geophysical datasets from the entire Caribbean region (Boschman et al., 2014) and the north-western Andes (Montes et al., 2019a, b), however, show very different motion paths for the Caribbean plate relative to SAM and a clear offset with the Galápagos hotspot at 90 Ma.

(Dobrovine et al., 2012). However, the geodynamic consistency of those models has been recently questioned, as they yield unreasonable velocities of slab advance and retreat and of global net rotation of the lithospheric plates (Müller et al., 2016; Schellart et al., 2008; Williams et al., 2015). Tetley et al. (2019) developed a data-optimized global absolute reference frame back to the Triassic that includes global hotspot track observations and estimates of net lithospheric rotation and paleo-trench migration. This geodynamically consistent absolute plate model is implemented in the latest global plate motion model of Müller et al. (2019), which also includes the detailed regional reconstructions of Boschman et al. (2014) for the Caribbean region, and thus corresponds to our “selected model” in the discussion below.

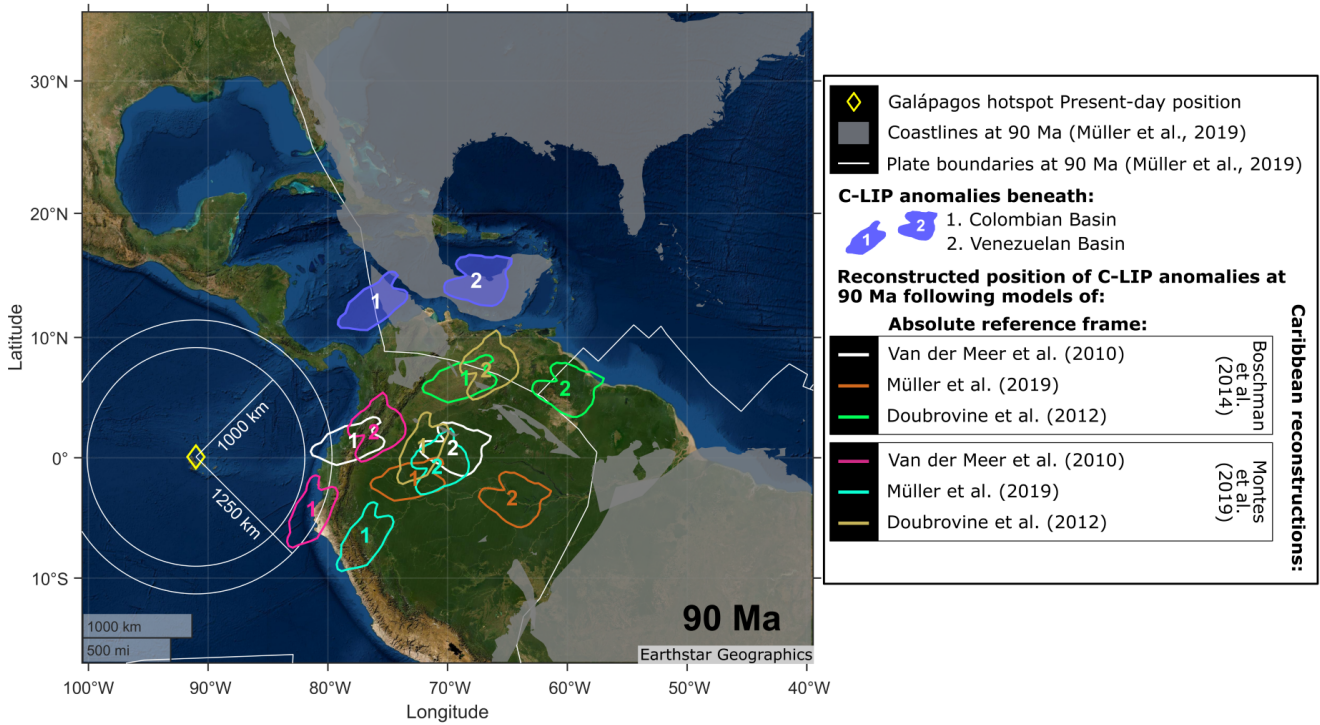
In this section, we aim to re-evaluate the hypothesis that the C-LIP (and interpreted preserved plume conduits) formed above the Galápagos hotspot by testing six different plate motion configurations using the GPlates software (Müller et al., 2018). We used the recently published regional plate kinematic models of Boschman et al. (2014) and Montes et al. (2019a), for which the rotation files are available, and three different absolute reference frames, i.e. the “subduction reference model” of Van Der Meer et al. (2010), the “Global Moving Hotspot model” of Dobrovine et al. (2012), and the

most recent “optimized global reference model” of Müller et al. (2019), as summarized in Table 3. The rotation files of all tested models are available as Supplement in Gómez-García et al. (2020) (see the data availability section below).

Figure 13a presents the results of the different kinematic reconstructions back to 90 Ma, using the polygons of the sub-crustal bodies in the Colombian and the Venezuelan basins (number 1 and 2, respectively). Here, white circles represent the plausible diameter of the plume head: 2000 km (Campbell, 2005) and 2500 km (Mauffret et al., 2001). Additionally, Fig. 13b depicts the motion paths of the centre of the Caribbean plateau since 90 Ma in absolute reference frame. In both figures, the present location of the Galápagos hotspot is represented by a yellow diamond at 0° N, 91° W (Nolet et al., 2019). The main outcome of these reconstructions is the clear offset between the C-LIP and the location of the hotspot at time of plateau formation (90 Ma) for all models, as previously reported by Boschman et al. (2014). In our selected model (Müller et al., 2019), the C-LIP centre was located ca. 2500 km to the east of the present-day Galápagos hotspot 90 Ma ago.

To evaluate the reasons behind this misfit, three possible sources of error should be discussed.

(a) Kinematic reconstructions of the positive mantle density anomalies at 90 Ma



(b) Motion paths of the centre of the C-LIP since 90 Ma

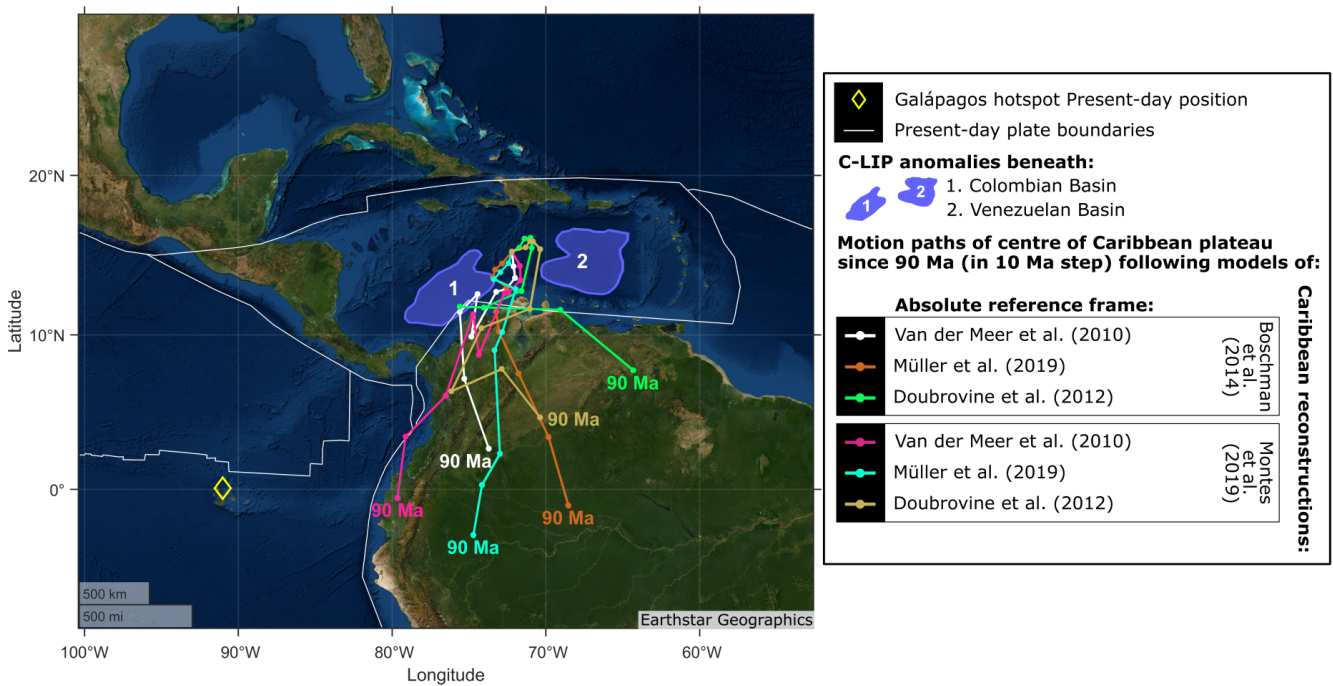


Figure 13. Kinematic reconstructions using three different absolute reference frames and two regional Caribbean reconstructions show an offset between the positive mantle density anomalies and the location of the Galápagos hotspot back to 90 Ma. (a) Reconstructions at 90 Ma using the plume conduits polygons beneath the Colombian and the Venezuelan basins (numbers 1 and 2, respectively). White circles represent the plausible head of the Galápagos plume assuming a 2000 and 2500 km diameter above a fixed plume. Present-day topography in the background for reference. (b) Motion paths of the centre of the C-LIP since 90 Ma (in 10 Ma steps). Different coloured lines depict the six different tested configurations.

Table 3. Summary of the kinematic models used to test the origin of the C-LIP in the Galápagos hotspot (0° N, 91° W; Nolet et al., 2019) and the corresponding distance to the centre of the Caribbean plateau at 90 Ma.

Regional kinematic model	Absolute reference frame		
	Van Der Meer et al. (2010) Distance from C-LIP centre at 90 Ma to present-day Galápagos hotspot (km)	Dobrovine et al. (2012)	Müller et al. (2019)
Boschman et al. (2014)	1946	3085	2505
Montes et al. (2019a)	1264	2352	1842

1. The exact paleo-location of the Caribbean plate relative to South America is still not well known, especially prior to ~ 67 Ma (age of development of arc magmatism in Panama; Montes et al., 2012), as shown by the differences between the regional reconstructions of Boschman et al. (2014) and Montes et al. (2019a). However, this difference between the regional reconstructions (ca. 750 km) is less significant than the offset between the C-LIP at 90 Ma and the present-day Galápagos hotspot, which ranges from 1264 to 3085 km, depending on the model used (ca. 2500 km for our selected model; Table 3).
2. The absolute motion of the tectonic plates can significantly change from one model to another. The smallest offsets between the centre of the C-LIP at 90 Ma and the present-day Galápagos hotspot (1264 and 1946 km, Table 3) are obtained with the subduction reference model of Van Der Meer et al. (2010). The largest offsets (2352–3085 km), on the other hand, are obtained with the Global Moving Hotspot model of Dobrovine et al. (2012). We note that previous authors have obtained a fit between the modern Galápagos hotspot and the C-LIP at 90 Ma using a fixed Pacific hotspots reference frame (Pindell and Kennan, 2009) and/or a docking of the Caribbean plate at 54.5 Ma (Nerlich et al., 2014). However, those models would require a larger differential motion of the Caribbean plate relative to South America than the motion described by Boschman et al. (2014) and Montes et al. (2019a). Moreover, as discussed above, those absolute reference frames are geodynamically inconsistent (e.g. Müller et al., 2016). Therefore, we would favour the optimized global reference frame of Müller et al. (2019) that yields an offset of 1842–2505 km between the paleo-C-LIP and the Galápagos hotspot at 90 Ma if the latter is considered fixed.
3. The (potential) migration of the Galápagos hotspot since 90 Ma is not considered in the tested absolute reference frames. However, it is difficult to reconstruct a motion for this hotspot as the track observed today associated with the Cocos and the Carnegie ridges is younger than 20 Ma (Werner et al., 2003). Nevertheless, strong geochemical evidence suggests a correlation between the C-LIP and the lavas of the present-day Galá-

pagos hotspot. Particularly, the Hf–Nd isotopic composition is interpreted as the Caribbean plateau representing the initial plume head of the Galápagos hotspot (i.e. Geldmacher et al., 2003; Thompson et al., 2004).

Steinberger and O’Connell (2000) proposed that the Easter Island hotspot migrated westward to south-westward at about $1\text{--}2\text{ cm yr}^{-1}$ in a mantle reference frame, due to return mantle flow from the Andean subduction zone. Thus, if we assume a similar migration velocity for the Galápagos hotspot since the establishment of the western Caribbean subduction beneath northern South America at about 67 Ma (age of arc magmatism in Panama, Montes et al., 2012), its paleo-position would be ca. 670–1340 km more to the east–north-east back in the Cretaceous period. If we subtract this motion from the offset of our selected model (2505 km, using Boschman et al., 2014, and Müller et al., 2019; Table 4), a residual offset of ca. 1165–1835 km between the migrated hotspot and the C-LIP remains. A fit between the C-LIP and the paleo-Galápagos would be obtained if we consider the possible large head of the plume during the large igneous province formation (e.g. 2000–2500 km in diameter; Campbell, 2005; Mauffret et al., 2001), as represented by the white circles in Fig. 13a.

To summarize, based on the argumentation above, the major offset between the paleo-position of the C-LIP at 90 Ma and the present-day Galápagos hotspot can be interpreted either as (1) the C-LIP having originated above the paleo-Galápagos hotspot only if this hotspot migrated significantly westward (> 1000 km at about $1\text{--}2\text{ cm yr}^{-1}$ in a mantle reference frame) since the establishment of the western Caribbean subduction and had a large plume head during the C-LIP formation (~ 2000 km diameter), or (2) the C-LIP having been formed by a different plume, which – if considered fixed – would nowadays be located below the South American continent (Fig. 13).

5.3 Implications for the tectonic development of the present-day Caribbean crust

The complex geologic development of the Caribbean crust involved volcanic mounds, sills, basalt flows, extensional episodes, and underplating of plume material (Driscoll and Diebold, 1999; Mauffret and Leroy, 1997), with heterogeneous, high-MgO rocks (up to 28 wt% MgO, Kerr, 2014).

The accreted portions of the C-LIP allowed the reconstruction of the geochemistry and temperature conditions that the mantle plume had at the time of the interaction with the Proto-Caribbean crust (Arndt et al., 1997; Hastie and Kerr, 2010; Kerr, 2005; Van Der Lelij et al., 2010; Neill et al., 2011). Indeed, the high-MgO rocks account for magmas that migrated relatively quickly from the mantle source (Kerr et al., 1998).

Geodynamic models support the evidence found in other large igneous plateaus related with a rapid, kilometre-scale uplift above the plume head. In these regions, the maximum uplift is also associated with lithospheric-scale extension in response to the buoyancy of the plume (e.g. Baes et al., 2016; Deng et al., 2014; François et al., 2018; He et al., 2003), and in most of the cases, the resulting crust is thicker than normal due to the magmatism above the plume head (Ernst, 2014). However, in the C-LIP history, the locations of the plume head and the associated uplift event(s) have been poorly constrained. Nevertheless, Diebold and Driscoll (1999) recognized that the extension and magmatism in the Caribbean were synchronous processes.

As seismic profiles of sufficient quality and spatial coverage are not freely available, 3D gravity models were used to assess the average crustal density configuration on a regional scale (Fig. 9). The average crustal densities highlight high-density areas affected by the plume interaction with the Proto-Caribbean crust, which significantly contributed to the thicker than normal crust that characterizes this plate (Diebold and Driscoll, 1999; Driscoll and Diebold, 1999; Edgar et al., 1971; Ewing et al., 1960; Mauffret and Leroy, 1997). This is in agreement with the early tectonic model of the Caribbean (Diebold and Driscoll, 1999; Driscoll and Diebold, 1999).

However, it is important to note the spatial correlation between the thin crust (< 10 km) reported by Mauffret and Leroy (1997) and the extended Proto-Caribbean crust both in the Colombian (Bowland and Rosencrantz, 1988) and the Venezuelan basins (Kroehler et al., 2011) with the subcrustal high-density bodies (Fig. 10). In the conventional tectonic model of the Caribbean of Diebold and Driscoll (1999), the C-LIP plume has been considered to be located below the thicker than normal crustal domains (see Fig. 11 in Driscoll and Diebold, 1999), whereas the relationship between the extended domains of the Colombian and the Venezuelan basins with the C-LIP evolution has not been well understood.

Geodynamic models show that the topographic uplift and subsidence patterns associated with the interaction of a mantle plume with the oceanic lithosphere could be of several kilometres, depending on factors such as the plume size, mantle and lithosphere rheology, and age of the overriding lithosphere (Burov and Cloetingh, 2009; François et al., 2018). Similarly, several studies suggest geological evidence of a rapid (~ 3 Ma) crustal doming prior to the eruption of basalts (e.g. Deng et al., 2014; He et al., 2003; Li et al., 2014; Zhang et al., 2016).

The previously described arguments led us to propose that the anomalously thin crust above the plume conduits in the Colombian and the Venezuelan basins corresponds to the centres of uplift. However, the lack of evidence that supports underplated material beneath these basins needs to be explained, and we hypothesize the following two options. (1) The magmatism occurred everywhere, but the uplifted part got eroded, as some geological evidence suggests for C-LIP-related subaerial volcanism (Buchs et al., 2018). Indeed, the erosion of the large igneous plateaus has been widely recognized in other plateaus worldwide, including extreme cases where the preserved structure includes areas with no basalts in the centre of the plume head (Ernst et al., 2005). (2) There was an offset between the plume head and the location of the basalt flows, and the magma paths were probably preferentially located along pre-existing lithospheric weakness zones (Buchan and Ernst, 2018; Ernst et al., 2019).

Based on the spatial correlation between the interpreted plume conduits and the extended crustal domains in the Colombian and the Venezuelan basins, we propose a modification to the tectonic model of the Caribbean, as described in Fig. 14. This cartoon is based on the tectonic model proposed by Driscoll and Diebold (1999) and on the present configuration of the Venezuelan Basin (Figs. 2, 13 and 14 in Diebold and Driscoll, 1999).

The initial configuration of the Proto-Caribbean crust consisted of a normal Farallon plate located in the eastern Pacific (Fig. 14a). In the Early Cretaceous, the plate started to interact with a mantle plume, creating rapid uplift and extension above the plume head (Fig. 14b). In the centre of uplift, extensional structures such as horst and grabens may have formed. Subsequently, the early stage basalts (ca. 90 Ma) spilled over the modified crust, preferentially flowing through predefined weakened regions accompanied by lateral and vertical redistribution of magmas (Ernst et al., 2019). In this stage, underplating of ultramafic cumulates started to contribute to the increase in crustal thickness (Fig. 14c). The lack of evidence for volcanism intruding the Proto-Caribbean domains of the Colombian and the Venezuelan basins today remains enigmatic (see the question marks in Fig. 14c). The thinning of the lithosphere above the plume head should be associated with decompression melting and magmatism, which to our knowledge have never been reported in those areas. Therefore, either the seismic reflection experiments have not been successful in mapping these structures, the basaltic flows were later eroded (Ernst, 2007, 2014), or the episodes of basalt flows took place only in the surrounding areas (with an offset of the plume head) along inherited weak portions of the lithosphere, as Ernst et al. (2019) proposed in their plumbing system model. Finally, a late stage (ca. 76 Ma) of magmatism may have reactivated the former plume conduits and/or formed new ones (Fig. 14d). The frozen plume conduits migrated together with the Caribbean plate from the Pacific, forming the present lithospheric configuration of the Caribbean plate, including the rough–smooth basement mor-

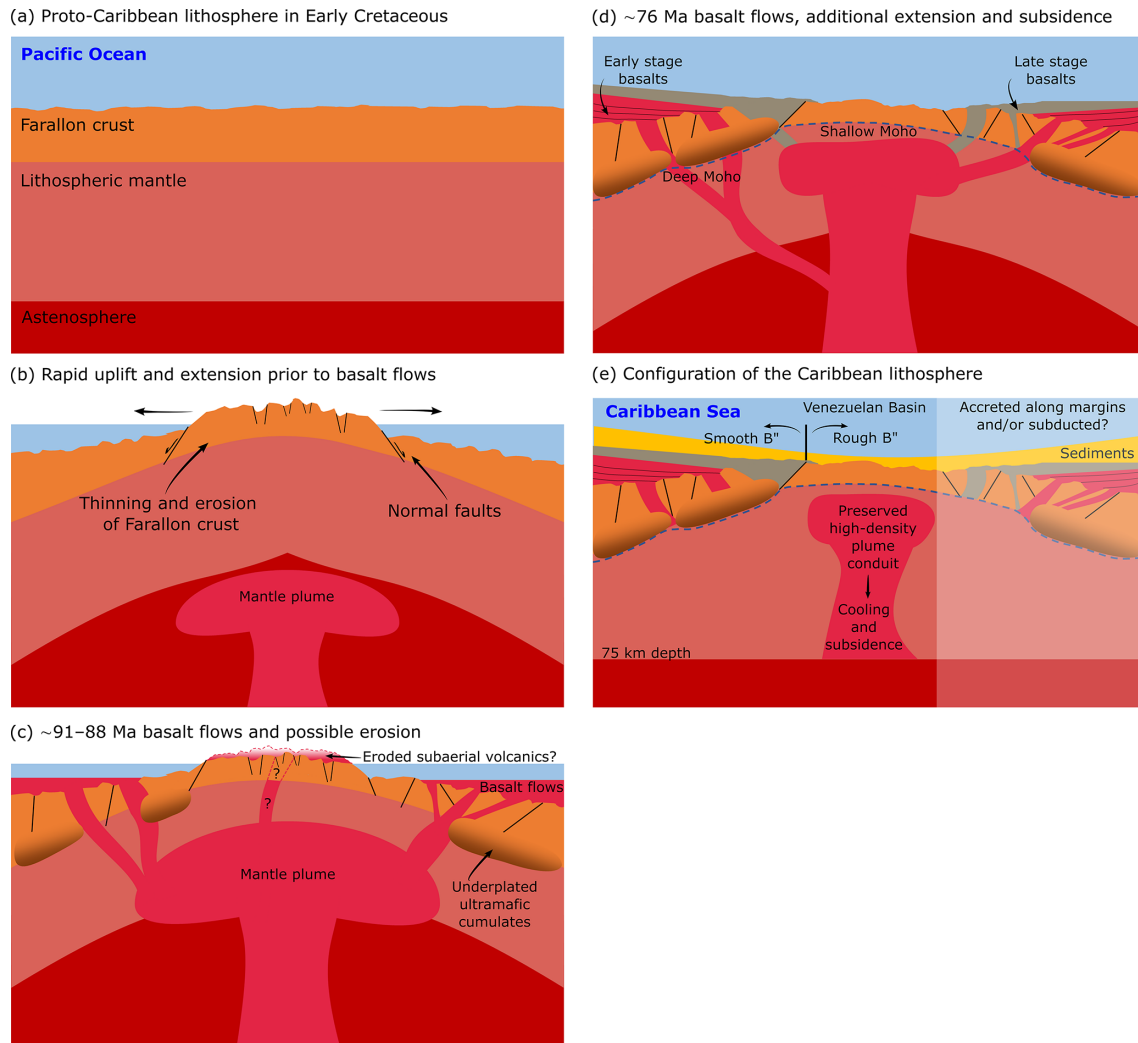


Figure 14. Cartoon illustrating the tectonic development of the Caribbean crust (Venezuelan Basin) due to the interaction of the Farallon plate with a mantle plume. **(a)** Proto-Caribbean lithosphere with a normal crustal thickness in the Early Cretaceous. **(b)** Rapid uplift and thinning of the lithosphere due to the inflow of hot, buoyant plume material. This stage should also have included the erosion of the uppermost crustal structures (e.g. Ernst, 2007, 2014) such as horsts and grabens associated with the stretching of the crust. Thus, only the main faults are preserved. **(c)** The early stage basalts are spilled over the modified Proto-Caribbean crust, probably including subaerial erosion of the ones spilled over the emerged portion of the crust. In this stage, the underplated ultramafic cumulates contributed to crustal thickening. Question marks indicate that the existence of magma conduits beneath the proposed centre(s) of uplift remains unclear. **(d)** The late basalts covered the crust, which experienced additional extension and subsidence. In this stage, a differential Moho depth becomes more evident. **(e)** In the present-day configuration of the Caribbean plate, the smooth basement (B'' horizon) is mainly preserved in the areas outside the uplift centre. The deepest Venezuelan and Colombian basins correlate with the most extended crustal domains, where the doming was more pronounced. Due to the north–north-eastward migration of the Proto-Caribbean plate, fragments of the C-LIP were subducted or accreted to the continental margins of the South American plate.

phology described by Driscoll and Diebold (1999). Parts of the C-LIP were accreted along the margins and/or subducted, and thus only the preserved lithosphere forms the Caribbean Sea nowadays (Fig. 14e).

In conclusion, the preserved extended Proto-Caribbean crust in the Colombian and the Venezuelan basins might account for the centres of (kilometre-scale) uplift. The plume-related high-density bodies present in the uppermost 75 km

of the Caribbean lithosphere may have contributed significantly to thermal subsidence of these basins, as suggested by the large water depths (up to 5 km) in the Venezuelan Basin (see Figs. 3a and 10, around 14° N and 66 – 68° W). Moreover, they might behave as rigid domains nowadays, affecting the overall behaviour of the Caribbean plate in response to regional tectonic stresses.

6 Conclusions

The 3D lithospheric-scale, data-integrative models of the Caribbean and north-western South American plates reveal density heterogeneities both in the crystalline crust and the upper mantle that are associated with the development of the C-LIP. The fitting of the measured gravity anomalies requires the presence of two relatively high-density (higher than the surroundings) subcrustal bodies, ranging between 3242 and 3300 kg m⁻³ (depending on their defined thickness a priori). These high-density domains can be followed down to 75 km depth, over approximately 400 km wide area, and are interpreted as the preserved, remaining material of the plume conduits responsible for the C-LIP formation. Such fossil plume conduit had never been identified before.

The observed two branches of high-density mantle might be related to the magma conduits of the two main pulses of magmatic activity, broadly recognized in the tectonic model of the C-LIP formation at ~91–88 and ~76 Ma. Assuming an S-wave velocity of 4540 ms⁻¹ as the boundary of the high-density mantle material, a total volume of ~12 × 10⁶ km³ is calculated for the Caribbean fossil plume. This volume is ~9 orders of magnitude higher than the excess magma volume reported by Kerr (2014) for the “in situ” plume material that currently forms the Caribbean crust. Nevertheless, future ocean bottom seismometer (OBS) campaigns would be required to obtain a more detailed image of the Caribbean upper mantle, providing new insights into the evolution of these intriguing, vast magmatic processes.

Surprisingly, the high-density anomalies are not found beneath the thick C-LIP crust and related basaltic flows but instead below the thinned Proto-Caribbean crust of the Colombian and the Venezuelan basins. We propose that these two areas underwent significant extension during uplift above the head of a rising mantle plume and that magmatism either took place mostly on the side of the plume head, possibly along pre-existing weakness zones in the lithosphere, or that magmatism was also present over these thinned domains but probably eroded in a subaerial environment.

Furthermore, the hypothesis that the C-LIP formed above the Galápagos plume was revisited. Kinematic reconstructions in an absolute reference frame show offsets in the range of ~1200 to 3000 km (depending on the model used) between the location of the C-LIP at the time of plateau formation (90 Ma) and the present-day Galápagos hotspot. These misfits suggest that either (1) the C-LIP originated above the paleo-Galápagos hotspot only if it migrated significantly westward (> 1000 km at about 1–2 cm yr⁻¹ in mantle reference frame) since the onset of the western Caribbean subduction and had a large plume head during the C-LIP formation (~2000 km diameter), or (2) the C-LIP was formed by a different plume, which – if considered fixed – would be nowadays located below the South American continent. Nevertheless, the existing strong geochemical evidence that supports the connection between the C-LIP and the Galápa-

gos hotspot favour the former and may highlight remaining pieces of the Caribbean “puzzle” that are not being considered in the kinematic models that are available nowadays.

Therefore, future efforts should focus on the improvement of the (1) imaging with more detail the structure of the Caribbean lithosphere, (2) plate-tectonic reconstructions of the Caribbean region and their relation with the probably not fixed Galápagos hotspot, and (3) testing plume–lithosphere interactions (cooling and motion of plume conduits with the lithosphere) with geodynamic models.

Finally, the workflow presented in this paper can be implemented in other plateaus worldwide as it relies on freely available, high-resolution geophysical information.

Data availability. The data to reproduce the results using the final model (M4, details in Sect. S1 of the Supplement) are available in Gómez-García et al. (2020, <https://doi.org/10.5880/GFZ.4.5.2020.003>). This data repository also includes the rotation files of the different kinematic reconstructions mentioned in this paper.

Supplement. The supplement related to this article is available online at: <https://doi.org/10.5194/se-12-275-2021-supplement>.

Author contributions. AMGG developed the initial research idea, carried out the collection, processing and integration of the data for the lithospheric structural and density models, plotted most of the figures, and wrote the initial draft of the manuscript. ELB carried out the kinematic reconstructions and most of the related figures. She also contributed to the literature review and the discussion of the manuscript. MSW and GM critically contributed with ideas during the development of the project, closely following the workflow steps and discussing the results. DA took part in the initial development of the structural models and contributed to the 3D visualization of the positive density anomalies and the figures related to the kinematic reconstructions. All the authors actively contributed to the revision and improvement of the draft version of the manuscript.

Competing interests. The authors declare that they have no conflict of interest.

Acknowledgements. We would like to thank Camilo Montes (Universidad del Norte) for the fruitful discussion about the GPLates reconstruction in the Caribbean. Ángela María Gómez-García is especially grateful to the EGU and the *Solid Earth* editorial board for their invitation to contribute as part of the OSPP award 2019. Thanks to Alejandro Mora (Hocol) for providing the shapefile of the Caribbean subduction and to Álvaro González (CRM, Barcelona) for the discussion regarding the tectonic development of the Caribbean. Ángela María Gómez-García was partially supported by COLCIENCIAS, Fundación para la Promoción de la

Investigación y la Tecnología, CEMARIN, and DAAD research grants.

Financial support. This research has been supported by the Departamento Administrativo de Ciencia, Tecnología e Innovación (COLCIENCIAS), the Fundación para la Promoción de la Investigación y la Tecnología (Project 4308), the CEMARIN, and the Deutscher Akademischer Austauschdienst (grant no. 91673157).

Review statement. This paper was edited by Caroline Beghein and reviewed by Richard Ernst and one anonymous referee.

References

- Álvarez, O., Nacif, S., Gimenez, M., Folguera, A., and Braitenberg, C.: GOCE derived vertical gravity gradient delineates great earthquake rupture zones along the Chilean margin, *Tectonophysics*, 622, 198–215, <https://doi.org/10.1016/j.tecto.2014.03.011>, 2014.
- Álvarez, O., Nacif, S., Spagnotto, S., Folguera, A., Gimenez, M., Chlieh, M., and Braitenberg, C.: Gradients from GOCE reveal gravity changes before Pisagua $M_w = 8.2$ and Iquique $M_w = 7.7$ large megathrust earthquakes, *J. S. Am. Earth Sci.*, 64, 273–287, <https://doi.org/10.1016/j.jsames.2015.09.014>, 2015.
- Amante, C. and Eakins, B. W.: ETOPO1 1 Arc-Minute Global Relief Model: Procedures, Data Sources and Analysis. NOAA Technical Memorandum NESDIS NGDC-24, National Geophysical Data Center, NOAA, <https://doi.org/10.7289/V5C8276M>, 2009.
- Arndt, N. T., Kerr, A. C., and Tarney, J.: Dynamic melting in plume heads: the formation of Gorgona komatiites and basalts, *Earth Planet. Sc. Lett.*, 146, 289–301, [https://doi.org/10.1016/S0012-821X\(96\)00219-1](https://doi.org/10.1016/S0012-821X(96)00219-1), 1997.
- Baes, M., Gerya, T., and Sobolev, S. V.: 3-D thermo-mechanical modeling of plume-induced subduction initiation, *Earth Planet. Sc. Lett.*, 453, 193–203, <https://doi.org/10.1016/j.epsl.2016.08.023>, 2016.
- Bernal-Olaya, R., Mann, P., and Vargas, C. A.: Earthquake, Tomographic, Seismic Reflection, and Gravity Evidence for a Shallowly Dipping Subduction Zone beneath the Caribbean Margin of Northwestern Colombia, *Pet. Geol. Potential Colomb. Caribb. Margin AAPG Mem.*, 108, 247–270, <https://doi.org/10.1306/13531939M1083642>, 2015.
- Bezada, M. J., Levander, A., and Schmandt, B.: Subduction in the southern Caribbean: Images from finite-frequency P wave tomography, *J. Geophys. Res.-Sol. Ea.*, 115, 1–19, <https://doi.org/10.1029/2010JB007682>, 2010.
- Blanco, J. F., Vargas, C. A., and Monsalve, G.: Lithospheric thickness estimation beneath Northwestern South America from an S-wave receiver function analysis, *Geochem. Geophys. Geosy.*, 18, 1376–1387, <https://doi.org/10.1002/2016GC006785>, 2017.
- Boschman, L. M., van Hinsbergen, D. J., Torsvik, T. H., Spakman, W., and Pindell, J. L.: Kinematic reconstruction of the Caribbean region since the Early Jurassic, *Earth-Sci. Rev.*, 138, 102–136, <https://doi.org/10.1016/j.earscirev.2014.08.007>, 2014.
- Bowland, C. L. and Rosencrantz, E.: Upper crustal structure of the western Colombian Basin, Caribbean Sea, *Geol. Soc. Am. Bull.*, 100, 534–546, [https://doi.org/10.1130/0016-7606\(1988\)100<0534:UCSOTW>2.3.CO;2](https://doi.org/10.1130/0016-7606(1988)100<0534:UCSOTW>2.3.CO;2), 1988.
- Brunet, D.: Implicit Contour Morphing Framework, available at: <http://www.mathworks.com/matlabcentral/fileexchange/66407-implicit-contour-morphing-framework> (last access: 17 August 2020), 2020.
- Brunet, D. and Sills, D.: An Implicit Contour Morphing Framework Applied to Computer-Aided Severe Weather Forecasting, *IEEE Signal Proc. Lett.*, 22, 1936–1939, <https://doi.org/10.1109/LSP.2015.2447279>, 2015.
- Buchan, K. L. and Ernst, R. E.: A giant circumferential dyke swarm associated with the High Arctic Large Igneous Province (HALIP), *Gondwana Res.*, 58, 39–57, <https://doi.org/10.1016/j.gr.2018.02.006>, 2018.
- Buchs, D. M., Kerr, A. C., Brims, J. C., Zapata-Villada, J. P., Correa-Restrepo, T., and Rodríguez, G.: Evidence for subaerial development of the Caribbean oceanic plateau in the Late Cretaceous and palaeo-environmental implications, *Earth Planet. Sc. Lett.*, 499, 62–73, <https://doi.org/10.1016/j.epsl.2018.07.020>, 2018.
- Burov, E. and Cloetingh, S.: Controls of mantle plumes and lithospheric folding on modes of intraplate continental tectonics: Differences and similarities, *Geophys. J. Int.*, 178, 1691–1722, <https://doi.org/10.1111/j.1365-246X.2009.04238.x>, 2009.
- Campbell, I. H.: Large Igneous Provinces and the Mantle Plume Hypothesis, *Elements*, 1, 265–269, <https://doi.org/10.2113/gselements.1.5.265>, 2005.
- Chiarabba, C., De Gori, P., Faccenna, C., Speranza, F., Seccia, D., Dionicio, V., and Prieto, G. A.: Subduction system and flat slab beneath the Eastern Cordillera of Colombia, *Geochem. Geophys. Geosy.*, 17, 16–27, <https://doi.org/10.1002/2015GC006048>, 2015.
- Christeson, G. L., Mann, P., Escalona, A., and Aitken, T. J.: Crustal structure of the Caribbean – Northeastern South America arc-continent collision zone, *J. Geophys. Res.-Sol. Ea.*, 113, 1–19, <https://doi.org/10.1029/2007JB005373>, 2008.
- Civiero, C., Armitage, J. J., Goes, S., and Hammond, J. O. S.: The Seismic Signature of Upper-Mantle Plumes: Application to the Northern East African Rift, *Geochem. Geophys. Geosy.*, 20, 6106–6122, <https://doi.org/10.1029/2019GC008636>, 2019.
- Deng, Y., Zhang, Z., Mooney, W., Badal, J., Fan, W., and Zhong, Q.: Mantle origin of the Emeishan large igneous province (South China) from the analysis of residual gravity anomalies, *Lithos*, 204, 4–13, <https://doi.org/10.1016/j.lithos.2014.02.008>, 2014.
- Diebold, J. and Driscoll, N.: Chapter 19 New insights on the formation of the Caribbean basalt province revealed by multi-channel seismic images of volcanic structures in the Venezuelan basin, *Sediment. Basins World*, 4, 561–568, 571–589 [https://doi.org/10.1016/S1874-5997\(99\)80053-7](https://doi.org/10.1016/S1874-5997(99)80053-7), 1999.
- Donnelly, T. W.: Magnetic anomaly observations in the Eastern Caribbean Sea, *Initial Reports Deep Sea Drill. Proj.*, 1023–1029, 1973.
- Dobrovine, P. V., Steinberger, B., and Torsvik, T. H.: Absolute plate motions in a reference frame defined by moving hot spots in the Pacific, Atlantic, and Indian oceans, *J. Geophys. Res.-Sol. Ea.*, 117, B09101, <https://doi.org/10.1029/2011JB009072>, 2012.

- Driscoll, N. and Diebold, J.: Chapter 20 Tectonic and stratigraphic development of the eastern Caribbean: New constraints from multichannel seismic data, *Sediment. Basins World*, 4, 591–595, 599–605, 611–626, [https://doi.org/10.1016/S1874-5997\(99\)80054-9](https://doi.org/10.1016/S1874-5997(99)80054-9), 1999.
- Duncan, R. A. and Hargraves, R. B.: Plate tectonic evolution of the Caribbean region in the mantle reference frame, in: *The Caribbean-South American Plate Boundary and Regional Tectonics* (Vol. 162), edited by: Bonini, W., Hargraves, R., and Shagam, R., Geological Society of America, <https://doi.org/10.1130/MEM162-p81>, 1984.
- Edgar, T., Ewing, J., and Hennion, J.: Seismic refraction and reflection in Caribbean Sea, *Am. Assoc. Petr. Geol.*, 55, 833–870, <https://doi.org/10.1306/819a3c76-16c5-11d7-8645000102c1865d>, 1971.
- Ernst, R. E.: Mafic-Ultramafic Large Igneous Provinces (LIPs): Importance of the Pre-Mesozoic record, *Episodes*, 30, 108–114, <https://doi.org/10.18814/epiuiugs/2007/v30i2/005>, 2007.
- Ernst, R. E.: *Large Igneous Provinces*, Cambridge University Press, Cambridge, <https://doi.org/10.1017/CBO9781139025300>, 2014.
- Ernst, R. E., Buchan, K. L., and Campbell, I. H.: Frontiers in Large Igneous Province research, *Lithos*, 79, 271–297, <https://doi.org/10.1016/j.lithos.2004.09.004>, 2005.
- Ernst, R. E., Liikane, D. A., Jowitt, S. M., Buchan, K. L., and Blanchard, J. A.: A new plumbing system framework for mantle plume-related continental Large Igneous Provinces and their mafic-ultramafic intrusions, *J. Volcanol. Geoth. Res.*, 384, 75–84, <https://doi.org/10.1016/j.jvolgeoes.2019.07.007>, 2019.
- Escalona, A. and Mann, P.: Tectonics, basin subsidence mechanisms, and paleogeography of the Caribbean-South American plate boundary zone, *Mar. Petrol. Geol.*, 28, 8–39, <https://doi.org/10.1016/j.marpetgeo.2010.01.016>, 2011.
- Ewing, J., Antoine, J., and Ewing, M.: Geophysical measurements in the Western Caribbean Sea and in the Gulf of Mexico, *J. Geophys. Res.*, 65, 4087–4126, <https://doi.org/10.1029/JZ065i012p04087>, 1960.
- EXXON: Tectonic map of the world, American Association of Petroleum Geologists Foundation, Tulsa, OK, 1985.
- Förste, C., Bruinsma, S., Abrikosov, O., Lemoine, J.-M., Marty, J.-C., Flechtner, F., Balmino, G., Barthelmes, F., and Biancale, R.: EIGEN-6C4 The latest combined global gravity field model including GOCE data up to degree and order 2190 of GFZ Potsdam and GRGS Toulouse, GFZ Data Serv., <https://doi.org/10.5880/icgem.2015.1>, 2014.
- François, T., Koptev, A., Cloetingh, S., Burov, E., and Gerya, T.: Plume-lithosphere interactions in rifted margin tectonic settings: Inferences from thermo-mechanical modelling, *Tectonophysics*, 746, 138–154, <https://doi.org/10.1016/j.tecto.2017.11.027>, 2018.
- Geldmacher, J., Hanan, B. B., Blichert-Toft, J., Harpp, K., Hornle, K., Hauff, F., Werner, R., and Kerr, A. C.: Hafnium isotopic variations in volcanic rocks from the Caribbean Large Igneous province and Galápagos hot spot tracks, *Geochem. Geophys. Geosy.*, 4, 1–24, <https://doi.org/10.1029/2002GC000477>, 2003.
- Goes, S., Govers, R., and Vacher, P.: Shallow mantle temperatures under Europe from P and S wave tomography, *J. Geophys. Res.-Earth*, 105, 11153–11169, <https://doi.org/10.1029/1999jb900300>, 2000.
- Gómez-García, A. M., Meeßen, C., Scheck-Wenderoth, M., Monsalve, G., Bott, J., Bernhardt, A., and Bernal, G.: Scripts to calculate the Vertical Gravity Gradients response of a 3D lithospheric model using spherical coordinates: the Caribbean oceanic domain as a case study, GFZ Data Services <https://doi.org/10.5880/GFZ.4.5.2019.002>, 2019a.
- Gómez-García, A. M., Meeßen, C., Scheck-Wenderoth, M., Monsalve, G., Bott, J., Bernhardt, A., and Bernal, G.: 3-D modeling of Vertical Gravity Gradients and the delimitation of tectonic boundaries: the Caribbean oceanic domain as a case study, *Geochem. Geophys. Geosy.*, 20, 5371–5393, <https://doi.org/10.1029/2019GC008340>, 2019b.
- Gómez-García, A. M., Le Breton, E., Scheck-Wenderoth, M., Monsalve, G., and Anikiev, D.: 3D lithospheric structure of the Caribbean and north South American plates and rotation files of kinematic reconstructions back to 90 Ma of the Caribbean Large Igneous Plateau, GFZ Data Services, <https://doi.org/10.5880/GFZ.4.5.2020.003>, 2020.
- Hacker, B. R. and Abers, G. A.: Subduction Factory 3: An Excel worksheet and macro for calculating the densities, seismic wave speeds, and H₂O contents of minerals and rocks at pressure and temperature, *Geochem. Geophys. Geosy.*, 5, 1–7, <https://doi.org/10.1029/2003GC000614>, 2004.
- Hastie, A. R. and Kerr, A. C.: Mantle plume or slab window?: Physical and geochemical constraints on the origin of the Caribbean oceanic plateau, *Earth-Sci. Rev.*, 98, 283–293, <https://doi.org/10.1016/j.earscirev.2009.11.001>, 2010.
- Hayes, G. P., Moore, G. L., Portner, D. E., Hearne, M., Flamme, H., Furtney, M., and Smoczyk, G. M.: Slab2, a comprehensive subduction zone geometry model, *Science*, 362, 58–61, <https://doi.org/10.1126/science.aat4723>, 2018.
- He, B., Xu, Y. G., Chung, S. L., Xiao, L., and Wang, Y.: Sedimentary evidence for a rapid, kilometer-scale crustal doming prior to the eruption of the Emeishan flood basalts, *Earth Planet. Sc. Lett.*, 213, 391–405, [https://doi.org/10.1016/S0012-821X\(03\)00323-6](https://doi.org/10.1016/S0012-821X(03)00323-6), 2003.
- Ince, E. S., Barthelmes, F., Reißland, S., Elger, K., Förste, C., Flechtner, F., and Schuh, H.: ICGEM – 15 years of successful collection and distribution of global gravitational models, associated services, and future plans, *Earth Syst. Sci. Data*, 11, 647–674, <https://doi.org/10.5194/essd-11-647-2019>, 2019.
- Kerr, A. C.: La Isla de Gorgona, Colombia: A petrological enigma?, *Lithos*, 84, 77–101, <https://doi.org/10.1016/j.lithos.2005.02.006>, 2005.
- Kerr, A. C.: Oceanic Plateaus, in: *Treatise on Geochemistry: Second Edition*, Vol. 4, 631–667, Oxford: Elsevier Ltd., <https://doi.org/10.1016/B978-0-08-095975-7.00320-X>, 2014.
- Kerr, A. C. and Mahoney, J. J.: Oceanic plateaus: Problematic plumes, potential paradigms, *Chem. Geol.*, 241, 332–353, <https://doi.org/10.1016/j.chemgeo.2007.01.019>, 2007.
- Kerr, A. and Tarney, J.: Tectonic evolution of the Caribbean and northwestern South America: The case for accretion of two Late Cretaceous oceanic plateaus, *Geology*, 33, 269–272, <https://doi.org/10.1130/G21109.1>, 2005.
- Kerr, A. C., Tarney, J., Saunders, A. D., Nivia, A., and Mariner, G. F.: The internal structure of oceanic plateaus: inferences from obducted Cretaceous terranes in western Colombia and the Caribbean, *Tectonophysics*, 292, 173–188, [https://doi.org/10.1016/S0040-1951\(98\)00067-5](https://doi.org/10.1016/S0040-1951(98)00067-5), 1998.

- Kroehler, M. E., Mann, P., Escalona, A., and Christeson, G. L.: Late Cretaceous-Miocene diachronous onset of back thrusting along the South Caribbean deformed belt and its importance for understanding processes of arc collision and crustal growth, *Tectonics*, 30, TC6003, <https://doi.org/10.1029/2011TC002918>, 2011.
- Laske, G., Masters, G., Ma, Z., and Pasyanos, M. E.: CRUST1.0: An Updated Global Model of Earth's Crust, *Geophys. Res. Abstr.*, EGU2013–2658, EGU General Assembly 2013, Vienna, Austria, 2013.
- Lewis, J. F., Kysar Mattiotti, G., Perfit, M., and Kamenov, G.: Geochemistry and petrology of three granitoid rock cores from the Nicaraguan rise, Caribbean sea: Implications for its composition, structure and tectonic evolution, *Geol. Acta*, 9, 467–479, <https://doi.org/10.1344/105.000001714>, 2011.
- Li, D., Yang, S., Chen, H., Cheng, X., Li, K., Jin, X., Li, Z., Li, Y., and Zou, S.: Late Carboniferous crustal uplift of the Tarim plate and its constraints on the evolution of the Early Permian Tarim Large Igneous Province, *Lithos*, 204, 36–46, <https://doi.org/10.1016/j.lithos.2014.05.023>, 2014.
- Mauffret, A. and Leroy, S.: Seismic stratigraphy and structure of the Caribbean igneous province, *Tectonophysics*, 283, 61–104, [https://doi.org/10.1016/S0040-1951\(97\)00103-0](https://doi.org/10.1016/S0040-1951(97)00103-0), 1997.
- Mauffret, A., Leroy, S., Vila, J. M., Hallot, E., de Lépinay Mercier, B., and Duncan, R. A.: Prolonged magmatic and tectonic development of the Caribbean Igneous Province revealed by a diving submersible survey, *Mar. Geophys. Res.*, 22, 17–45, <https://doi.org/10.1023/A:1004873905885>, 2001.
- McNutt, M. and Caress, D. W.: Crust and Lithospheric Structure – Hot Spots and Hot-Spot Swells, in: *Treatise on Geophysics*, Vol. 1, 445–478, Elsevier B.V., Oxford, <https://doi.org/10.1016/B978-0-444-53802-4.00212-8>, 2007.
- Meeßen, C.: VelocityConversion, GFZ Data Services, <https://doi.org/10.5880/GFZ.6.1.2017.001>, 2017.
- Monsalve, G., Jaramillo, J. S., Cardona, A., Schulte-Pelkum, V., Posada, G., Valencia, V., and Poveda, E.: Deep crustal faults, shear zones, and magmatism in the Eastern Cordillera of Colombia: growth of a plateau from teleseismic receiver function and geochemical Mio-Pliocene volcanism constraints, *J. Geophys. Res.-Sol. Ea.*, 124, 9833–9851, <https://doi.org/10.1029/2019JB017835>, 2019.
- Montelli, R., Nolet, G., Dahlen, F. A., Masters, G., Engdahl, E. R., and Hung, S. H.: Finite-Frequency Tomography Reveals a Variety of Plumes in the Mantle, *Science*, 303, 338–343, <https://doi.org/10.1126/science.1092485>, 2004.
- Montes, C., Bayona, G., Cardona, A., Buchs, D. M., Silva, C. A., Morón, S., Hoyos, N., Ramírez, D. A., Jaramillo, C. A., and Valencia, V.: Arc-continent collision and orocline formation: Closing of the Central American seaway, *J. Geophys. Res.-Sol. Ea.*, 117, 1–25, <https://doi.org/10.1029/2011JB008959>, 2012.
- Montes, C., Rodríguez-Corcho, A. F., Bayona, G., Hoyos, N., Zapata, S., and Cardona, A.: Continental margin response to multiple arc-continent collisions: The northern Andes-Caribbean margin, *Earth-Sci. Rev.*, 198, 102903, <https://doi.org/10.1016/j.earscirev.2019.102903>, 2019a.
- Montes, C., Rodríguez-Corcho, A. F., Bayona, G., Hoyos, N., Zapata, S., and Cardona, A.: GPlates dataset for the tectonic reconstruction of the Northern Andes-Caribbean Margin, *Data Br.*, 25, 104398, <https://doi.org/10.1016/j.dib.2019.104398>, 2019b.
- Mora-Bohórquez, J. A., Ibáñez-Mejía, M., Oncken, O., de Freitas, M., Vélez, V., Mesa, A., and Serna, L.: Structure and age of the Lower Magdalena Valley basin basement, northern Colombia: New reflection-seismic and U-Pb-Hf insights into the termination of the central Andes against the Caribbean basin, *J. S. Am. Earth Sci.*, 74, 1–26, <https://doi.org/10.1016/j.jsames.2017.01.001>, 2017.
- Mora, J. A., Oncken, O., Le Breton, E., Ibáñez-Mejía, M., Faccenna, C., Veloza, G., Vélez, V., de Freitas, M., and Mesa, A.: Linking Late Cretaceous to Eocene tectonostratigraphy of the San Jacinto fold belt of NW Colombia with Caribbean plateau collision and flat subduction, *Tectonics*, 36, 2599–2629, <https://doi.org/10.1002/2017TC004612>, 2017.
- Müller, R. D., Seton, M., Zahirovic, S., Williams, S. E., Matthews, K. J., Wright, N. M., Shephard, G. E., Maloney, K. T., Barnett-Moore, N., Hosseinpour, M., Bower, D. J., and Cannon, J.: Ocean Basin Evolution and Global-Scale Plate Reorganization Events Since Pangea Breakup, *Annu. Rev. Earth Pl. Sc.*, 44, 107–138, <https://doi.org/10.1146/annurev-earth-060115-012211>, 2016.
- Müller, R. D., Cannon, J., Qin, X., Watson, R. J., Gurnis, M., Williams, S., Pfaffelmoser, T., Seton, M., Russell, S. H. J., and Zahirovic, S.: GPlates: Building a Virtual Earth Through Deep Time, *Geochem. Geophys. Geosy.*, 19, 2243–2261, <https://doi.org/10.1029/2018GC007584>, 2018.
- Müller, R. D., Zahirovic, S., Williams, S. E., Cannon, J., Seton, M., Bower, D. J., Tetley, M. G., Heine, C., Le Breton, E., Liu, S., Russell, S. H. J., Yang, T., Leonard, J., and Gurnis, M.: A Global Plate Model Including Lithospheric Deformation Along Major Rifts and Orogens Since the Triassic, *Tectonics*, 38, 1884–1907, <https://doi.org/10.1029/2018TC005462>, 2019.
- Neill, I., Kerr, A. C., Hastie, A. R., Stanek, K.-P., and Millar, I. L.: Origin of the Aves Ridge and Dutch-Venezuelan Antilles: interaction of the Cretaceous “Great Arc” and Caribbean-Colombian Oceanic Plateau?, *J. Geol. Soc. London*, 168, 333–348, <https://doi.org/10.1144/0016-76492010-067>, 2011.
- Nerlich, R., Clark, S. R., and Bunge, H. P.: Reconstructing the link between the Galapagos hotspot and the Caribbean Plateau, *GeoresJ*, 1–2, 1–7, <https://doi.org/10.1016/j.grj.2014.02.001>, 2014.
- Nolet, G., Hello, Y., Lee, S. van der, Bonniex, S., Ruiz, M. C., Pazmino, N. A., Deschamps, A., Regnier, M. M., Font, Y., Chen, Y. J., and Simons, F. J.: Imaging the Galápagos mantle plume with an unconventional application of floating seismometers, *Sci. Rep.*, 9, 1–12, <https://doi.org/10.1038/s41598-018-36835-w>, 2019.
- O'Neill, C., Müller, D., and Steinberger, B.: On the uncertainties in hot spot reconstructions and the significance of moving hot spot reference frames, *Geochem. Geophys. Geosy.*, 6, Q04003, <https://doi.org/10.1029/2004GC000784>, 2005.
- Pindell, J. and Kennan, L.: Tectonic evolution of the Gulf of Mexico, Caribbean and northern South America in the mantle reference frame: an update, edited by: James, K. H., Lorente, M. A., and Pindell, J. L., *Orig. Evol. Caribb. plate. Geol. Soc. London, Spec. Publ.*, 328, 1–55, <https://doi.org/10.1144/SP328.1>, 2009.
- Pindell, J., Kennan, L., Stanek, K. P., Maresch, W. V., and Draper, G.: Foundations of Gulf of Mexico and Caribbean evolution: Eight controversies resolved, *Geol. Acta*, 4, 303–341, <https://doi.org/10.1144/SP328.1>, 2006.

- Pindell, J. L. and Barrett, S. F.: Geological evolution of the Caribbean region; A Plate tectonic perspective, in: *The Geology of North America*, edited by: Dengo, G. and Case, J. E., 405–432, Geological Society of America, Boulder, Colorado, <https://doi.org/10.1130/DNAG-GNA-H.405>, 1990.
- Porritt, R. W., Becker, T. W., and Monsalve, G.: Seismic anisotropy and slab dynamics from SKS splitting recorded in Colombia, *Geophys. Res. Lett.*, 41, 8775–8783, <https://doi.org/10.1002/2014GL061958>, 2014.
- Reguzzoni, M. and Sampietro, D.: GEMMA: An Earth crustal model based on GOCE satellite data, *Int. J. Appl. Earth Obs.*, 35, 31–43, <https://doi.org/10.1016/j.jag.2014.04.002>, 2015.
- Rosencrantz, E.: Structure and tectonics of the Yucatan Basin, Caribbean Sea, as determined from seismic reflection studies, *Tectonics*, 9, 1037–1059, <https://doi.org/10.1029/TC009i005p01037>, 1990.
- Sæther, B.: Improved estimation of subsurface magnetic properties using minimum mean-square error methods, Norwegian University of Science and Technology, Trondheim, 1997.
- Sanchez-Rojas, J. and Palma, M.: Crustal density structure in north-western South America derived from analysis and 3-D modeling of gravity and seismicity data, *Tectonophysics*, 634, 97–115, <https://doi.org/10.1016/j.tecto.2014.07.026>, 2014.
- Schaeffer, A. J. and Lebedev, S.: Global shear speed structure of the upper mantle and transition zone, *Geophys. J. Int.*, 194, 417–449, <https://doi.org/10.1093/gji/ggt095>, 2013.
- Schellart, W. P., Stegman, D. R., and Freeman, J.: Global trench migration velocities and slab migration induced upper mantle volume fluxes: Constraints to find an Earth reference frame based on minimizing viscous dissipation, *Earth-Sci. Rev.*, 88, 118–144, <https://doi.org/10.1016/j.earscirev.2008.01.005>, 2008.
- Schmidt, S., Plonka, C., Götze, H. J., and Lahmeyer, B.: Hybrid modelling of gravity, gravity gradients and magnetic fields, *Geophys. Prospect.*, 59, 1046–1051, <https://doi.org/10.1111/j.1365-2478.2011.00999.x>, 2011.
- Sinton, C. W., Duncan, R. A., Storey, M., Lewis, J., and Estrada, J. J.: An oceanic flood basalt province within the Caribbean plate, *Earth Planet. Sc. Lett.*, 155, 221–235, [https://doi.org/10.1016/s0012-821x\(97\)00214-8](https://doi.org/10.1016/s0012-821x(97)00214-8), 1998.
- Siravo, G., Faccenna, C., Gérard, M., Becker, T. W., Fellin, M. G., Herman, F., and Molin, P.: Slab flattening and the rise of the Eastern Cordillera, Colombia, *Earth Planet. Sc. Lett.*, 512, 100–110, <https://doi.org/10.1016/j.epsl.2019.02.002>, 2019.
- Steinberger, B. and O’Connell, R. J.: Effects of mantle flow on hotspot motion, *Geophys. Monogr. Ser.*, 121, 377–398, <https://doi.org/10.1029/GM121p0377>, 2000.
- Steinberger, B. and Torsvik, T. H.: Absolute plate motions and true polar wander in the absence of hotspot tracks, *Nature*, 452, 620–623, <https://doi.org/10.1038/nature06824>, 2008.
- Syracuse, E. M., Maceira, M., Prieto, G. A., Zhang, H., and Ammon, C. J.: Multiple plates subducting beneath Colombia, as illuminated by seismicity and velocity from the joint inversion of seismic and gravity data, *Earth Planet. Sc. Lett.*, 444, 139–149, <https://doi.org/10.1016/j.epsl.2016.03.050>, 2016.
- Tetley, M. G., Williams, S. E., Gurnis, M., Flament, N., and Müller, R. D.: Constraining Absolute Plate Motions Since the Triassic, *J. Geophys. Res.-Sol. Ea.*, 124, 7231–7258, <https://doi.org/10.1029/2019JB017442>, 2019.
- Thompson, P. M. E., Kempton, P. D., White, R. V., Kerr, A. C., Tarney, J., Saunders, A. D., Fitton, J. G., and McBirney, A.: Hf-Nd isotope constraints on the origin of the Cretaceous Caribbean plateau and its relationship to the Galápagos plume, *Earth Planet. Sc. Lett.*, 217, 59–75, [https://doi.org/10.1016/S0012-821X\(03\)00542-9](https://doi.org/10.1016/S0012-821X(03)00542-9), 2004.
- Uieda, L., Oliveira Jr., V. C., and Barbosa, V. C. F.: Modeling the Earth with Fatiando a Terra, in: *Proceedings of the 12th Python in Science Conference*, edited by: van der Walt, S., Millman, J., and Huff, K., 96–103, Austin, Texas, <https://doi.org/10.25080/majora-8b375195-010>, 2013.
- Van Benthem, S., Govers, R., Spakman, W., and Wortel, R.: Tectonic evolution and mantle structure of the Caribbean, *J. Geophys. Res.-Sol. Ea.*, 118, 3019–3036, <https://doi.org/10.1002/jgrb.50235>, 2013.
- Van Der Lelij, R., Spikings, R. A., Kerr, A. C., Kounov, A., Cosca, M., Chew, D., and Villagomez, D.: Thermochronology and tectonics of the Leeward Antilles: Evolution of the southern Caribbean Plate boundary zone, *Tectonics*, 29, TC6003, <https://doi.org/10.1029/2009TC002654>, 2010.
- Van Der Meer, D. G., Spakman, W., Van Hinsbergen, D. J. J., Amaru, M. L., and Torsvik, T. H.: Towards absolute plate motions constrained by lower-mantle slab remnants, *Nat. Geosci.*, 3, 36–40, <https://doi.org/10.1038/ngeo708>, 2010.
- Vargas, C. A. and Mann, P.: Tearing and breaking off of subducted slabs as the result of collision of the Panama arc-indenter with Northwestern South America, *B. Seismol. Soc. Am.*, 103, 2025–2046, <https://doi.org/10.1785/0120120328>, 2013.
- Wagner, L. S., Jaramillo, J. S., Ramírez-Hoyos, L. F., Monsalve, G., Cardona, A., and Becker, T. W.: Transient slab flattening beneath Colombia, *Geophys. Res. Lett.*, 44, 6616–6623, <https://doi.org/10.1002/2017GL073981>, 2017.
- Watts, A. B., Ten Brink, U. S., Buhl, P., and Brocher, T. M.: A multichannel seismic study of lithospheric flexure across the Hawaiian-Emperor seamount chain, *Nature*, 315, 105–111, <https://doi.org/10.1038/315105a0>, 1985.
- Weatherall, P., Marks, K. M., Jakobsson, M., Schmitt, T., Tani, S., Arndt, J. E., Rovere, M., Chayes, D., Ferrini, V., and Wigley, R.: A new digital bathymetric model of the world’s oceans, *Earth Space Sci.*, 2, 331–345, <https://doi.org/10.1002/2015EA000107>, 2015.
- Werner, R., Hoernle, K., Barckhausen, U., and Hauff, F.: Geodynamic evolution of the Galápagos hot spot system (Central East Pacific) over the past 20 m.y.: Constraints from morphology, geochemistry, and magnetic anomalies, *Geochem. Geophys. Geosy.*, 4, 1108, <https://doi.org/10.1029/2003GC000576>, 2003.
- Wessel, P. and Kroenke, L. W.: Pacific absolute plate motion since 145 Ma: An assessment of the fixed hot spot hypothesis, *J. Geophys. Res.-Sol. Ea.*, 113, 1–21, <https://doi.org/10.1029/2007JB005499>, 2008.
- Williams, S., Flament, N., Dietmar Müller, R., and Butterworth, N.: Absolute plate motions since 130 Ma constrained by subduction zone kinematics, *Earth Planet. Sc. Lett.*, 418, 66–77, <https://doi.org/10.1016/j.epsl.2015.02.026>, 2015.
- Yarce, J., Monsalve, G., Becker, T. W., Cardona, A., Poveda, E., Alvira, D., and Ordoñez-Carmona, O.: Seismological observations in Northwestern South America: Evidence for two subduction segments, contrasting crustal thick-

nesses and upper mantle flow, *Tectonophysics*, 637, 57–67, <https://doi.org/10.1016/j.tecto.2014.09.006>, 2014.

Zhang, S. H., Zhao, Y., Ye, H., and Hu, G. H.: Early Neoproterozoic emplacement of the diabase sill swarms in the Liaodong Peninsula and pre-magmatic uplift of the southeastern North China Craton, *Precambrian Res.*, 272, 203–225, <https://doi.org/10.1016/j.precamres.2015.11.005>, 2016.